Phonons and their Coupling to Magnons in $n = 2$ Ruddlesden-Popper Compounds.

A. B. Harris

Department of Physics and Astronomy,

University of Pennsylvania, Philadelphia PA 19104

(Dated: January 26, 2011)

Abstract

The number of absorption and Raman optical modes for each Wyckoff orbit in the high-temperature tetragonal (I4/mmm) parent lattice of the Ruddlesden-Popper compounds $Ca_3X_2O_7$, with X=Mn or X=Ti is given. We analyze the effect of sequential perturbations which lower the symmetry to Cmcm and Cmc2$_1$ and finally include magnetic ordering. We determine the power law behavior (within mean field theory) for the cross section for photon absorption and Raman scattering of modes which appear as the symmetry is successively lowered. In the Cmc2$_1$ phase we give a symmetry analysis to discuss the magnon-phonon coupling which in other systems gives rise to "electromagnons." From our results we suggest several experiments to clarify the phase diagram and other properties of these systems.

I. INTRODUCTION

The Ruddlesden-Popper (RP) compounds[1] are those of the type $A_{n+1}B_n$ C_{3n+1}, where the valences of the ions are A = +2, B = +4, and C = −2 (usually C is oxygen). At high temperature the crystal structure for many of these compounds is tetragonal, but the structure can distort in several ways as the temperature passes through structural phase transitions. In the lowest symmetry phase, these systems are usually ferroelectric and can also be magnetically ordered, although, in contrast to many magnetoelectrics,[2–7] these two degrees of freedom do not appear at the same temperature. Nevertheless the RP systems do have many interesting couplings between their magnetic and dielectric properties. For example, their spontaneous polarization can be rotated by the application of a magnetic field and the weak ferromagnetic moment can be rotated by the application of an electric field.[8,9] The symmetry of the RP's is very similar to that of the Aurivillius compound $SrBi_2Ta_2O_9$ analyzed in detail by Perez-Mato *et al.*[10] and many of our results should also apply to it. Although there have been several first principles calculations of the properties of CMO and/or CTO,[8,11,12] the calculations of CF are most relevant to the present paper.

FIG. 1: (Color online) The tetragonal phase of CMO or CTO (space group I4/mmm). The oxygen ions are the blue spheres, the Ca ions are the open green circles, and the Mn or Ti ions (not shown) are at the centers of the octahedra of oxygen ions. There are two molecules per conventional unit cell.
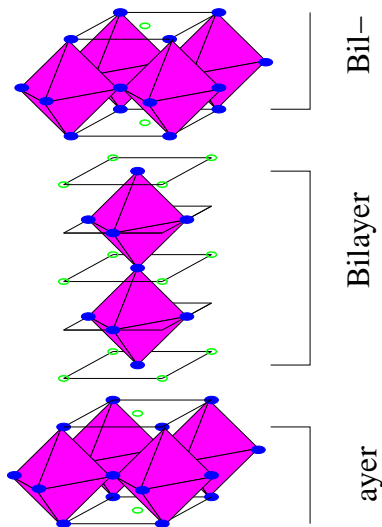
Here we will be interested in the two RP compounds $Ca_3Mn_2O_7$ (CMO) and $Ca_3Ti_2O_7$ (CTO)

(CTO), which consist of bilayers of oxygen octahedra enclosing a Mn or Ti ion. It is believed that the high-temperature phase is tetragonal (I4/mmm)[13,14] and the low-temperature phase is orthorhombic (Cmc2$_1$)[15] and in Fig. 2 we show the three possible paths that connect these structures.[8] First principles calculations[8] indicate that the most likely scenario involves the appearance, as the temperature is lowered, of the intermediate state Cmcm at a temperature we denote $T_>$. In fact, the Cmcm phase has been observed in the isostructural compounds LaCa$_2$Mn$_2$O$_7$[16] at and below room temperature and Bi$_{0.44}$Ca$_{2.56}$Mn$_2$O$_7$[17] at room teperature. Accordingly, we will assume that this scenario applies to CMO and CTO although for these systems no intermediate phase has been observed up to now. However, recent measurements on ceramic CMO find a clear pyroelectric signal consistent with the onset of ferroelectric order close to $T_> = 280$K.[18] This transition is identified as the temperature at which Cmc2$_1$ appears. Since this ferroelectric transition seems to be a continuous and well-developed one and since a direct continuous transition between I4/mmm and Cmc2$_1$ is inconsistent with Landau theory,[19] the seemingly inescapable conclusion is that the phase for T slightly greater than $T_>$ is *not* I4/mmm, but is some phase which does not allow a spontaneous polarization. Thus the phase at temperature just above $T_>$ may be the Cmcm phase. In this scenario the Cmc2$_1$ phase would appear at a lower temperature $T_<$ (which experimental data implies is quite close to $T_>$). The purpose of the present paper is to discuss the symmetry of the zone center phonons and the Raman scattering cross section as they are modified by the successive lowering of symmetry as the temperature is reduced through the structural phase transitions at $T_>$ and $T_<$. Such a symmetry analysis can be done using standard group theory methods. Here we will supplement that analysis with an analysis of the phonon cross sections from which we determine their power law dependence on the order parameters (OP's) which characterize the distortions from tetragonal symmetry to the lower symmetry structures. This enables us to predict the temperature dependence of the newly allowed cross sections which appear at the structural phase transitions. We then give a similar analysis of the magnon-phonon interaction. As a result of this coupling, the magnon absorption cross section (which usually results from a magnetic dipole allowed transition) is enhanced by now being electric-dipole allowed. This enhancement has led some authors[20–25] to call such magnons "electromagnons."

Briefly, this paper is organized as follows. In Sec. II we give a symmetry analysis of the zone center phonons in the tetragonal (I4/mmm) phase and in Secs. III and IV

3

we give similar analyses for the orthorhombic Cmcm and Cmc2$_1$ phases. We discuss the photon absorption and Raman scattering of these modes. For modes which only appear as a consequence of a phase transition we also determine the power-law dependence of their optical cross sections on the emergent OP's. In Sec. V we discuss the coupling of these modes to magnetic excitations (magnons). Our results are summarized in Sec. VI.
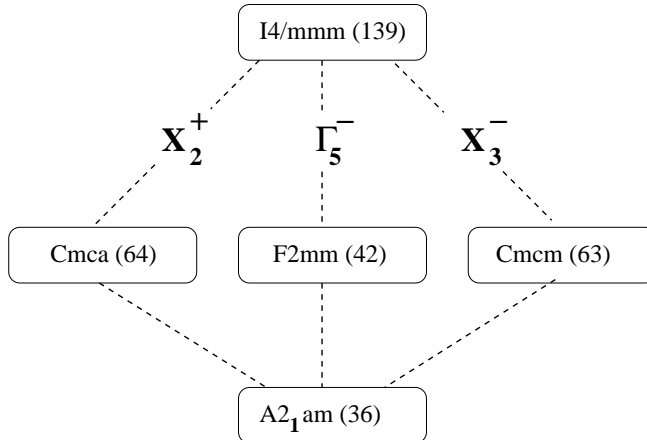

FIG. 2: The group-subgroup structure of CMO and CTO. We indicate the irreducible representations (irreps) by which the tetragonal phase is distorted to reach one of the intermediate phases. The numbering of the space groups follows Ref. 26. The superscripts on the irreps give the parity with respect to spatial inversion. The irrep Γ_5^- is at zero wave vector and the X irreps are at the wave vectors $\mathbf{q} = (1/2, \pm 1/2, 0)$. In the final step to reach the A2$_1$am (equivalent to Cmc2$_1$) structure the other two irreps are introduced simultaneously,[9] so that Cmc2$_1$ can be regarded as the result of simultaneous condensation of the three irreps.

II.   SYMMETRY ANALYSIS FOR THE TETRAGONAL STRUCTURE

The occupied sites in space group I4/mmm for the $n = 2$ RP system are given in the first three columns of Table III, below. The character table for the little group of $\mathbf{q} = 0$ for the I4/mmm tetragonal structure is given in Table I. For the one dimensional irreducible representations (irreps) the characters are the matrices. For the two dimensional irreps and for the irreps for the X points at $\mathbf{q} = (1/2, \pm 1/2, 0)$ (in rlu's) the matrices are given in Table II.[28]

TABLE I: Character table for the little group of $\mathbf{q} = 0$ for the I4/mmm tetragonal structure. The operator numbers are those of Ref. 27. The bottom row gives the dipole moment vector $\mathbf{P}$ or the Raman tensor $\mathbf{R}$, where a, b, c, etc. are arbitrary constants. For the two dimensional irreps the two entries are the values of $\mathbf{P}$ and $\mathbf{R}$ for each of the two degenerate states. The entry is left blank for irreps which are optically inactive.

Number	Operator	Γ_1^+	Γ_2^+	Γ_3^+	Γ_4^+	Γ_5^+	Γ_1^-	Γ_2^-	Γ_3^-	Γ_4^-	Γ_5^-
1	(xyz)	1	1	1	1	2	1	1	1	1	2
37,40	$(yxz),(\overline{y},\overline{x},z)$	1	-1	-1	1	0	-1	1	1	-1	0
4	$(\overline{x}\overline{y}z)$	1	1	1	1	-2	1	1	1	1	-2
3,2	$(\overline{x}y\overline{z}),(x\overline{y}\overline{z})$	1	1	-1	-1	0	1	1	-1	-1	0
39,38	$(\overline{y}x\overline{z}),(y\overline{x}\overline{z})$	1	-1	1	-1	0	-1	1	-1	1	0
25	$(\overline{x}\overline{y}\overline{z})$	1	1	1	1	2	-1	-1	-1	-1	-2
13,16	$(\overline{y}\overline{x}\overline{z}),(yx\overline{z})$	1	-1	-1	1	0	1	-1	-1	1	0
28	$(xy\overline{z})$	1	1	1	1	-2	-1	-1	-1	-1	2
27,26	$(x\overline{y}z),(\overline{x}yz)$	1	1	-1	-1	0	-1	-1	1	1	0
15,14	$(y\overline{x}z),(\overline{y}xz)$	1	-1	1	-1	0	1	-1	1	-1	0
P		$a(\hat{i}\hat{i}+\hat{j}\hat{j})$	$c(\hat{i}\hat{i}$		$d(\hat{i}\hat{j}$	$e(\hat{i}\hat{k}+\hat{k}\hat{i})$			$g\hat{k}$		$h\hat{i}$
or **R**		$+b\hat{k}\hat{k}$	$-\hat{j}\hat{j})$		$+\hat{j}\hat{i})$	$e(\hat{j}\hat{k}+\hat{k}\hat{j})$					$h\hat{j}$

We now discuss briefly the introduction of order parameters (OP's). Starting from the high-temperature tetragonal, I4/mmm, structure, distortions of the irreps Γ_5^-, X_3^- and X_2^+ are condensed as the temperature is lowered to eventually reach the low-symmetry low-temperature Cmc2$_1$ structure. A tabulation of these symmetry-adapted distortion vectors, $\Psi_n^{(X)}$, for irrep X is given in Table III. In the dominant component of the distortion of irrep X_2^+ the octahedra are rotated about the crystal c axis like interlocking gears. The rotations in the upper $(z = \tau)$ and lower $(z = -\tau)$ planes of a bilayer are equal, so in the notation of Refs. 29 and 30 these rotations are both denoted $(0, 0, \Theta)$. The dominant component of the distortion of irrep X_3^- consists of 1) a rotation about the tetragonal [1,0,0] with the rotation alternating in sign as one moves along the [1,0,0] direction and 2) a rotation about the tetragonal [0,1,0] direction with the rotation alternating in sign as one moves along the

TABLE II: Representation matrices $M^{(\mathbf{G})}(\mathcal{O})$ for the operators $\mathcal{O}$ which are the generators of the irrep $\mathbf{G}$. Here $\mathbf{r}' = \mathcal{O}\mathbf{r}$ and the $\boldsymbol{\sigma}$'s are the Pauli matrices. For the irreps $\mathbf{G}$ at zero wave vector the matrices for the translations $\mathbf{T}_1 \equiv (x+1, y, z)$, $\mathbf{T}_2 \equiv (x, y+1, z)$, and $\mathbf{T}_3 \equiv (x+\frac{1}{2}, y+\frac{1}{2}, z-\frac{1}{2})$ are unity. For the irreps at the $\mathbf{X}$ wave vectors the matrices are $\mathbf{M}(\mathbf{T}_1) = \mathbf{M}(\mathbf{T}_2) = -\mathbf{1}$ and $\mathbf{M}(\mathbf{T}_3) = -\sigma_z$. The first row and column for the $\mathbf{X}$ irreps refer to wave vector $\mathbf{q}_1$ These matrices are related to those of Ref. 19 by a unitary transformation which, for zero wave vector takes $(\boldsymbol{\sigma}_x, \boldsymbol{\sigma}_y, \boldsymbol{\sigma}_z)$ into $(-\boldsymbol{\sigma}_x, -\boldsymbol{\sigma}_y, \boldsymbol{\sigma}_z)$ and for the wave vector $\mathbf{X}$ takes $(\boldsymbol{\sigma}_x, \boldsymbol{\sigma}_y, \boldsymbol{\sigma}_z)$ into $(-\boldsymbol{\sigma}_z, \boldsymbol{\sigma}_y, -\boldsymbol{\sigma}_x)$.

$\mathcal{O} =$	$\mathcal{R}_4$	m_d	m_z
$\mathbf{r}' =$	$(\overline{y}, x, z)$	(y, x, z)	$(x, y, \overline{z})$
$\mathbf{M}^{(\mathbf{X}_1^+)}(\mathcal{O}) =$	$-\boldsymbol{\sigma}_x$	1	$\mathbf{1}$
$\mathbf{M}^{(\mathbf{X}_2^+)}(\mathcal{O}) =$	$\boldsymbol{\sigma}_x$	-1	$\mathbf{1}$
$\mathbf{M}^{(\mathbf{X}_3^+)}(\mathcal{O}) =$	$-i\boldsymbol{\sigma}_y$	$\boldsymbol{\sigma}_z$	-1
$\mathbf{M}^{(\mathbf{X}_4^+)}(\mathcal{O}) =$	$i\boldsymbol{\sigma}_y$	$-\boldsymbol{\sigma}_z$	-1
$\mathbf{M}^{(\mathbf{X}_1^-)}(\mathcal{O}) =$	$-\boldsymbol{\sigma}_x$	-1	-1
$\mathbf{M}^{(\mathbf{X}_2^-)}(\mathcal{O}) =$	$\boldsymbol{\sigma}_x$	1	-1
$\mathbf{M}^{(\mathbf{X}_3^-)}(\mathcal{O}) =$	$-i\boldsymbol{\sigma}_y$	$-\boldsymbol{\sigma}_z$	1
$\mathbf{M}^{(\mathbf{X}_4^-)}(\mathcal{O}) =$	$i\boldsymbol{\sigma}_y$	$\boldsymbol{\sigma}_z$	1
$\mathbf{M}^{(\Gamma_5^-)}(\mathcal{O}) =$	$i\boldsymbol{\sigma}_y$	$\boldsymbol{\sigma}_x$	1
$\mathbf{M}^{(\Gamma_5^+)}(\mathcal{O}) =$	$i\boldsymbol{\sigma}_y$	$\boldsymbol{\sigma}_x$	-1

[0,1,0] direction. Since this distortion is an even function of z, we identify this distortion as $(\Phi, \Phi, 0)$ in the upper layer and $(-\Phi, -\Phi, 0)$ in the lower layer.

If we assume that the distortions are small, then the crystal structure in any of the phases can be approximated as a distortion from the tetragonal structure which is written as linear combination of the distortions of the three irreps listed in Table III:

$$\Phi = \sum_{m,X} Q_m^{(X)} \Psi_m^{(X)} ,$$

where $\Psi_m^{(X)}$ is the 12 component vector of irrep X as in Table III. Since the notation to distinguish the various irreps which we will encounter is somehwat complicated, we summarize the notation in Table IV. If we regard the basis vectors $\Psi_m^{(X)}$ as fixed, then application

6

TABLE III: Basis functions $\Psi_1^{(X)}$ and $\Psi_2^{(X)}$ for the distortion under irrep X, where $X = 5, 3, 2$ indicates irrep Γ_5^-, X_3^-, and X_2^+, respectively.[28] For each site we give the three components of the vector displacement. We assume normalization so that the sum of the squares of the components is unity. The values of the structural parameters are given in Ref. 13: $\rho = 0.311$, $\xi = 0.100$, $\chi = 0.205$, and $\tau = 0.087$. Since the a and b sites have the same symmetry we will refer to them both as a sites.

Site	n	$\mathbf{r}$	$\Psi_{1,n}^{(5)}$	$\Psi_{2,n}^{(5)}$	$\Psi_{1,n}^{(3)}$	$\Psi_{2,n}^{(3)}$	$\Psi_{1,n}^{(2)}$	$\Psi_{2,n}^{(2)}$
A sites								
e	1	$(0,0,\rho+1/2)$	u 0 0	0 u 0	a $-a$ 0	$-a$ $-a$ 0	0 0 0	0 0 0
e	2	$(0,0,-\rho+1/2)$	u 0 0	0 u 0	a $-a$ 0	$-a$ $-a$ 0	0 0 0	0 0 0
b	3	$(0,0,1/2)$	v 0 0	0 v 0	b $-b$ 0	$-b$ $-b$ 0	0 0 0	0 0 0
B sites								
e	4	$(0,0,\xi)$	w 0 0	0 w 0	c $-c$ 0	$-c$ $-c$ 0	0 0 0	0 0 0
e	5	$(0,0,-\xi)$	w 0 0	0 w 0	c $-c$ 0	$-c$ $-c$ 0	0 0 0	0 0 0
O sites								
a	6	$(0,0,0)$	x 0 0	0 x 0	d $-d$ 0	$-d$ $-d$ 0	0 0 0	0 0 0
e	7	$(0,0,\chi)$	y 0 0	0 y 0	e $-e$ 0	$-e$ $-e$ 0	0 0 0	0 0 0
e	8	$(0,0,-\chi)$	y 0 0	0 y 0	e $-e$ 0	$-e$ $-e$ 0	0 0 0	0 0 0
g	9	$(0,1/2,\tau)$	z_1 0 0	0 z_2 0	0 0 f	0 0 f	$-h$ $-g$ 0	$-h$ g 0
g	10	$(0,1/2,-\tau)$	z_1 0 0	0 z_2 0	0 0 $-f$	0 0 $-f$	$-h$ $-g$ 0	$-h$ g 0
g	11	$(1/2,0,\tau)$	z_2 0 0	0 z_1 0	0 0 $-f$	0 0 f	g h 0	$-g$ h 0
g	12	$(1/2,0,-\tau)$	z_2 0 0	0 z_1 0	0 0 f	0 0 $-f$	g h 0	$-g$ h 0

of an operator $\mathcal{O}$ in the symmetry group of the tetragonal space group to Φ will induce a transformation of the OP's as [9]

$$\mathcal{O}Q_m^{(X)} = \sum_k M_{k,m}^{(X)}(\mathcal{O})Q_k^{(X)} \, ,$$

where the representation matrices $\mathbf{M}^{(X)}(\mathcal{O})$ for the all the relevant operators $\mathcal{O}$ can be constructed from those given for the generators of the irrep X given in Table II. This equation defines the symmetry of the OP's.

TABLE IV: Notation for order parameters. First column: full notation, subsequent column(s): abbreviated notation.

For	Full	Abbrev	Abrev'
$m = 1, 2$	$Q_m^{(\Gamma_5^-)}$	$\equiv Q_5^-(m)$	$\equiv Q_5(m)$
$m = 1, 2$	$Q_m^{(\Gamma_5^+)}$	$\equiv Q_5^+(m)$	
$p < 5$	$Q_1^{(\Gamma_p^-)}$	$\equiv Q_p^-(0)$	
$p < 5$	$Q_1^{(\Gamma_p^+)}$	$\equiv Q_p^+(0)$	
	$[Q_1^{(\Gamma_5^-)} + Q_2^{(\Gamma_5^-)}]\sqrt{2} \equiv$	$Z^- \equiv$	Z
	$[Q_1^{(\Gamma_5^-)} - Q_2^{(\Gamma_5^-)}]\sqrt{2} \equiv$	$Y^- \equiv$	Y
	$[Q_1^{(\Gamma_5^+)} + Q_2^{(\Gamma_5^+)}]/\sqrt{2} \equiv$	Z^+	
	$[Q_1^{(\Gamma_5^+)} - Q_2^{(\Gamma_5^+)}]/\sqrt{2} \equiv$	Y^+	
	$Q_1^{(\Gamma_3^-)}$	$\equiv Q_3^-(0) \equiv$	X
$m = 1, 2$	$Q_m^{(X_2^+)}$	$\equiv Q_2^+(\mathbf{q}_m) \equiv Q_2(\mathbf{q}_m)$	
$m = 1, 2$	$Q_m^{(X_3^-)}$	$\equiv Q_3^-(\mathbf{q}_m) \equiv Q_3(\mathbf{q}_m)$	
$m = 1, 2, p \neq 2$	$Q_m^{(X_p^+)}$	$\equiv Q_p^+(\mathbf{q}_m)$	
$m = 1, 2, p \neq 3$	$Q_m^{(X_3^-)}$	$\equiv Q_3^-(\mathbf{q}_m)$	

As explained in Ref. 9 these distortions form two families, one of which involves wave vector $\mathbf{q}_1 \equiv (1/2, 1/2, 0)$ and the other of which involves wave vector $\mathbf{q}_2 \equiv (1/2, -1/2, 0)$.[31] The wave vectors $(1/2, \pm 1/2, 0)$ correspond to a doubling of the size of the primitive unit cell. The first family is described by the three OP's $Q_3^-(\mathbf{q}_1)$, $Q_2^+(\mathbf{q}_1)$, and $Z \propto Q_1^{(\Gamma_5^-)} + Q_2^{(\Gamma_5^-)}$, and the second by the OP's $Q_3^-(\mathbf{q}_2)$, $Q_2^+(\mathbf{q}_2)$, and $Y \propto Q_1^{(\Gamma_5^-)} - Q_2^{(\Gamma_5^-)}$. In the absence of any external fields, when the sample orders, one expects an equal population of domains of the two families. However, it is possible to select a single family by invoking the coupling[9]

$$V = a\epsilon_{xy}[Q_k(\mathbf{q}_1)^2 - Q_k(\mathbf{q}_2)^2] , \tag{1}$$

where ϵ_{xy} is a shear component of strain, and $k = 2$ or 3. One can utilize this interaction by cooling the sample through $T_>$ in the presences of a shear stress conjugate to ϵ_{xy}. This will preferentially select $\mathbf{q}_1$ or $\mathbf{q}_2$, depending on the sign of the stress and the sign of the constant a. It is possible that the selection of the wave vector can also be accomplished by cooling in an electric or magnetic field.[9]

Our aim is describe the evolution of the cross section for a) zero wave vector photon absorption and b) Raman scattering in terms of the various OP's.

The single photon absorption process results from the electromagnetic coupling $V_E = -\mathbf{p} \cdot \mathbf{E}$, where $\mathbf{E}$ is the electric field of the incident electromagnetic wave and $\mathbf{p}$ is the dipole moment operator of the system. The symmetry indicated in Tables I and II indicates that in the tetragonal phase one has

$$p_x = a_x Q_5(1) , \quad p_y = a_y Q_5(2) , \quad p_z = a_z Q_3^-(0) ,$$

with $a_y = a_x$. Note: in reality we ought to index the modes by an additional index to distinguish between different modes of the same symmetry. Thus, for instance,

$$p_x = \sum_{k=1}^{n(\Gamma_5^-)} a_{k,x} Q_5(1)_k , \tag{2}$$

where $n(\Gamma_5^-)$ is the number of occurrences of Γ_5^-, which, in this case, is [see Eq. (4), below] $n(\Gamma_5^-) = 7$. For simplicity we will usually not display this index explicitly, but in all our results sums over such an index (or indices) are implied. We discuss the use of Eq. (2) in Appendix A. The absorption cross section is proportional to the square of the scalar product of the polarization vector of the incident photon and the dipole moment vector for the irrep in question.[32,33] (For the two dimensional irrep one has to sum the squares of the two scalar products.)

Likewise, the Raman scattering process results from the electromagnetic coupling $V_E = -\sum_{\beta\gamma} \alpha_{\beta\gamma} E_\beta E_\gamma$, where $\boldsymbol{\alpha}$ is the polarizability tensor, which depends on the phonon displacements as

$$\alpha_{\beta\gamma} = \alpha_{\beta\gamma}^{(0)} + \sum_\tau \frac{\partial \alpha_{\beta\gamma}}{\partial Q_\tau} Q_\tau .$$

We consider the cross section (or intensity) for a process in which the incident photon has an electric field vector in the β direction and the scattered photon has an electric field vector in the γ direction (we call this the β-γ polarization) and a phonon Q_τ is created (or destroyed). The cross section for this process is proportional to the square of the tensor product of the Raman tensor $\partial \alpha_{\beta\gamma}/\partial Q_\tau$ with the polarizations of the incoming and outgoing photons.[32,33] (For the two dimensional irreps one sums these squares over the two states of the irreps.) For both absorption and scattering we implicitly assume that the photon wave length is very large in comparison to the size of the unit cell.

Now we determine which modes (at zero wave vector) are allowed in the tetragonal lattice. Using standard methods we find that the reducible representations Γ corresponding to the space of zero wave vector displacements of the Wyckoff orbits a, e, and g, are decomposed into their irreps as

$$
\begin{aligned}
\Gamma(a) &= \Gamma_5^- + \Gamma_3^- ,\\
\Gamma(e) &= \Gamma_5^- + \Gamma_3^- + \Gamma_5^+ + \Gamma_1^+ ,\\
\Gamma(g) &= 2\Gamma_5^- + \Gamma_4^- + \Gamma_3^- + 2\Gamma_5^+ + \Gamma_2^+ + \Gamma_1^+ ,
\end{aligned}
\tag{3}
$$

so that the reducible representation Γ corresponding to the space of the vector displacements of all 12 ions in the primitive unit cell has the decomposition into irreps as

$$
\begin{aligned}
\Gamma &= 2\Gamma(a) + 3\Gamma(e) + \Gamma(g) = 7\Gamma_5^- + \Gamma_4^-\\
&\quad + 6\Gamma_3^- + 5\Gamma_5^+ + 4\Gamma_1^+ + \Gamma_2^+ .
\end{aligned}
\tag{4}
$$

The allowed absorption modes [x and y from $\Gamma_5^-(0)$ and z from $\Gamma_3^-(0)$] are listed in Table V. Thus we find that in the tetragonal phase there are 20 absorption modes, 6 from Γ_3^- which have z polarization and 7 pairs of doubly degenerate modes (one with x polarization and one with y polarization) coming from Γ_5^-. Note that of these 20 absorption modes three are acoustic (zero frequency) and are not observed in IR experiments. There are also 15 Raman active modes, five nondegenerate modes coming from irreps Γ_1^+ and Γ_2^+ and 5 pairs of doubly degenerate modes coming from Γ_5^+. Because the lowest symmetry sites of the space group I4/mmm are not occupied in CMO or CTO, it happens that there are no modes for which the Raman polarization xy is nonzero. Indeed, this result can be used as a signature of the tetragonal phase of CTO or CMO.

III. ORTHORHOMBIC SPACE GROUP CMCM (# 63)

A. Analysis based on Cmcm symmetry

We now consider the modifications in the optical spectrum when we condense irrep X_3^- at wave vector $\mathbf{q}_1 = (1/2, 1/2, 0)$ to go into the space group Cmcm. The transformation from tetragonal to orthorhombic coordinates is illustrated in Fig. 3 and is given by

$$
X_O = z_t, \qquad Y_O = \frac{x_t - y_t}{2} - \frac{1}{4},
$$

10

TABLE V: Number of modes Q of the tetragonal phase with their polarizations x, y, or z, for Wyckoff orbits, RP(n) for $n = a, b, c$. The phonon modes $Q_5^{\pm}(1)$ and $Q_5^{\pm}(2)$ are degenerate in energy. To identify with modes in the orthorhombic phase $z_t \to X_O$, $(x_t, y_t) \to (Y_O, Z_O)$, where the subscript O (t) refers to the orthorhombic (tetragonal) coordinate system. Pol. denotes polarization in a notation where xy indicates that the Raman tensor is $\mathbf{R} = \text{const}(\hat{i}\hat{j} + \hat{j}\hat{i})$, $X_O Y_O$ indicates that $\mathbf{R} = \text{const}(\hat{I}\hat{J} + \hat{J}\hat{I})$, where lower case unit vectors are tetragonal and capitals are orthorhombic, and similarly for other polarizations. Also $Y_O^2 - Z_O^2$ indicates that $\mathbf{R} = \text{const.}(\hat{J}\hat{J} - \hat{K}\hat{K})$ and X_O^2, $(Y_O^2 + Z_O^2)$ indicates that $\mathbf{R} = a\hat{I}\hat{I} + b(\hat{J}\hat{J} + \hat{K}\hat{K})$, where a and b are constants. (The orthorhombic polarizations are those when the tetragonal symmetry is broken.) The row labeled TOT gives the total number of modes for 2 a orbits, 3 e orbits, and 1 g orbit.

	Absorption			Raman Scattering				
Mode$_t$	$Q_5^-(1)$	$Q_5^-(2)$	$Q_3^-(0)$	$Q_5^+(1)$	$Q_5^+(2)$	$Q_4^+(0)$	$Q_2^+(0)$	$Q_1^+(0)$
Pol.$_t$	x	y	z	zx	zy	xy	$x^2 - y^2$	$x^2 + y^2, z^2$
Mode$_O$	Y	Z	X	Y^+	Z^+			
Pol.$_O$	Y	Z	X	XY	XZ	$(Y^2 - Z^2)$	YZ	$X^2, (Y^2 + Z^2)$
RP(a)	1	1	1	0	0	0	0	0
RP(e)	1	1	1	1	1	0	0	1
RP(g)	2	2	1	2	2	0	1	1
TOT[a]	7	7	6	5	5	0	1	4

a) Here and below the absorption modes include an acoustic mode for each polarization.

$$Z_O = \frac{x_t + y_t}{2} - \frac{1}{4}, \tag{5}$$

where here and below we use lower case letters for tetragonal coordinates and capitals for orthorhombic coordinates. The O unit cell is twice as large as the t unit cell. That is why $x_t \pm y_t$ is divided by 2 rather than by $\sqrt{2}$. In Table VI we give the character table for the little group of $\mathbf{q} = 0$ for Cmcm as well as the characters for the reducible representation associated with the vector displacement over each of the Wyckoff orbits.

To find out how many Cmcm optically active modes there are, we need to convert the tetragonal coordinates into the orthorhombic coordinates but we do not need to explicitly
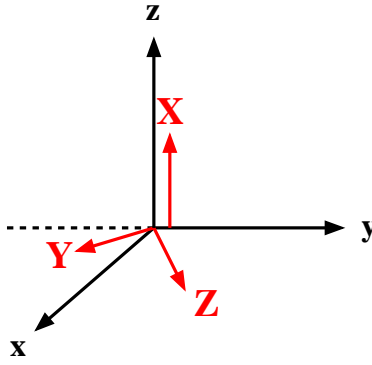
11

FIG. 3: (Color online) Tetragonal (large black arrows) and orthorhombic (small red arrows) axes.

TABLE VI: Character table for the little group of $\mathbf{q} = 0$ for Cmcm and (in the last row) how they transform. The last three columns give the character vectors for displacements for the Wyckoff orbits of the RP lattice. The Γ_1^+ modes are Raman active with Raman tensor $\mathbf{R} = a\hat{I}\hat{I} + b\hat{J}\hat{J} + c\hat{K}\hat{K}$. All coordinates are orthorhombic. The modes of irrep Γ_3^- transform like XYZ and are silent.

Class	Operator	Γ_1^+	Γ_2^+	Γ_3^+	Γ_4^+	Γ_1^-	Γ_2^-	Γ_3^-	Γ_4^-	a	e	g
E	(X, Y, Z)	1	1	1	1	1	1	1	1	6	12	24
2_X	$(X, \overline{Y}, \overline{Z})$	1	-1	1	-1	1	-1	1	-1	0	0	-8
m_Z	$(X, Y, \frac{1}{2} - Z)$	1	-1	-1	1	1	-1	-1	1	2	4	0
m_Y	$(X, \overline{Y}, \frac{1}{2} + Z)$	1	1	-1	-1	1	1	-1	-1	0	0	0
$\mathcal{I}$	$(\overline{X}, \overline{Y}, \overline{Z})$	1	1	1	1	-1	-1	-1	-1	0	0	0
m_X	$(\overline{X}, Y, Z)$	1	-1	1	-1	-1	1	-1	1	2	0	0
2_Z	$(\overline{X}, \overline{Y}, \frac{1}{2} + Z)$	1	-1	-1	1	-1	1	1	-1	0	0	0
2_Y	$(\overline{X}, Y, \frac{1}{2} - Z)$	1	1	-1	-1	-1	-1	1	1	-2	0	0
P or **R**		1	XZ	YZ	XY	X	Z	XYZ	Y			

include the distortion that makes the orthorhombic structure. From the parent tetragonal orbit a we have the orthorhombic orbit

$$\mathbf{r}_1 = (0, 0, 0)_t = (0, -\frac{1}{4}, -\frac{1}{4})_o \ ,$$

$$\mathbf{r}_2 = (1, 0, 0)_t = (0, \frac{1}{4}, \frac{1}{4})_o \ ,$$

where the subscript t means tetragonal and the subscript o means Cmcm. We find that

$$\Gamma(a_{Cmcm}) = \Gamma_1^+ + \Gamma_3^+ + \Gamma_4^+ + \Gamma_1^- + \Gamma_2^- + \Gamma_4^- \ . \tag{6}$$

For the parent tetragonal orbit e we have

$$\mathbf{r}_1 = (0,0,z)_t = (z, -\frac{1}{4}, -\frac{1}{4})_o \ ,$$

$$\mathbf{r}_2 = (1,0,z)_t = (z, \frac{1}{4}, \frac{1}{4})_o \ ,$$

$$\mathbf{r}_3 = (0,0,-z)_t = (-z, -\frac{1}{4}, -\frac{1}{4})_o \ ,$$

$$\mathbf{r}_4 = (1,0,-z)_t = (-z, \frac{1}{4}, \frac{1}{4})_o \ ,$$

and we find that

$$\Gamma(e_{Cmcm}) = 2\Gamma_1^+ + \Gamma_2^+ + \Gamma_3^+ + 2\Gamma_4^+ + 2\Gamma_1^- + \Gamma_2^-$$

$$+\Gamma_3^- + 2\Gamma_4^- \ . \tag{7}$$

Similarly, for the parent tetragonal orbit g we find that

$$\Gamma(g_{Cmcm}) = 2\Gamma_1^+ + 4\Gamma_2^+ + 2\Gamma_3^+ + 4\Gamma_4^+ + 2\Gamma_1^-$$

$$+4\Gamma_2^- + 2\Gamma_3^- + 4\Gamma_4^- \ . \tag{8}$$

Thus the decomposition of the reducible representation for the displacements of all ions in the unit cell is

$$\Gamma = 2\Gamma(a_{Cmcm}) + 3\Gamma(e_{Cmcm}) + \Gamma(g_{Cmcm})$$

$$= 10\Gamma_1^+ + 7\Gamma_2^+ + 7\Gamma_3^+ + 12\Gamma_4^+ + 10\Gamma_1^-$$

$$+9\Gamma_2^- + 5\Gamma_3^- + 12\Gamma_4^- \ .$$

So in the Cmcm phase we have 10 modes with X_O polarization, 12 modes with Y_O polarization, and 9 modes with Z_O polarization, as given in Table VII. (The degeneracies of the tetragonal structure are removed in the Cmcm structure.) Results for the Raman-active modes are also given in Table VII.

B.   Analysis based on lowering of tetragonal symmetry

We now discuss the phonon modes by analyzing the perturbative effect of distortions from the tetragonal parent structure. Compared to the previous analysis, this analysis provides

13

TABLE VII: As Table V. Modes Q in the orthorhombic Cmcm phase for the Wyckoff orbits descended from the tetragonal orbits. The irreps $\Gamma_n^\pm$ are those of Table VI for the Cmcm phase. In the next to last row we give the total number of modes for 2 a orbits, 3 e orbits and 1 g orbit. In the last row we repeat the results for the total number of modes for the tetragonal system.

	Absorption			Raman			
IRREP	Γ_1^-	Γ_2^-	Γ_4^-	Γ_1^+	Γ_2^+	Γ_3^+	Γ_4^+
Polarization	X_O	Z_O	Y_O	X_O^2, Y_O^2, Z_O^2	$X_O Z_O$	$Y_O Z_O$	$X_O Y_O$
RP(a)	1	1	1	1	0	1	1
RP(e)	2	1	2	2	1	1	2
RP(g)	2	4	4	2	4	2	4
TOT	10	9	12	10	7	7	12
TET	6	7	7	4	5	1	5

information on how the intensity of the new Cmcm modes depends on the amplitude of the orthorhombic distortion from tetragonal symmetry. Let us suppose that $Q_3^-(\mathbf{q}_1)$ has condensed due to the phase transition at temperature $T = T_>$ into the Cmcm phase. (Near this phase transition one can choose modes so that only a single mode of this symmetry is involved. As the temperature is lowered below $T_>$ other modes of this symmetry will progressively be introduced.) To see how the existence of the new order parameter can modify modes of the tetragonal system consider the Hamiltonian $\mathcal{H}_5$ for $Q_{5,n}^-$,

$$\mathcal{H}_5 = \frac{1}{2}\kappa_5\left(Q_5(1)^2 + Q_5(2)^2\right) + \frac{1}{2}\kappa_{3-}[Q_3^-(\mathbf{q}_1)]^2$$
$$+ \sum_n b_n Q_5(1)Q_5(2)\langle Q_3^-(\mathbf{q}_1)\rangle^n , \qquad (9)$$

where the κ's are stiffnesses and we put angled brackets around $Q_3(\mathbf{q}_1)$ to indicate that these higher than quadratic terms give rise to effective quadratic terms written here when $Q_3^-(\mathbf{q}_1)$ (whose value minimizes the free energy) is regarded as the constant $\langle Q_3^-(\mathbf{q}_1)\rangle$. To make the above Hamiltonian invariant under all the operations of the parent tetragonal system, we would have to include analogous terms involving $\mathcal{R}_4 Q_3^-(\mathbf{q}_1) = Q_3^-(\mathbf{q}_2)$, where $\mathbf{q}_2 = (1/2, -1/2, 0)$. However, since we are considering a scenario in which $Q_3^-(\mathbf{q}_2)$ is zero, we do not need to write these terms here. Since $b_1 = 0$ due to wave vector conservation, Eq.

(9) is

$$\mathcal{H}_5 = \frac{1}{2}\left(\kappa_5 - b_2\langle Q_3^-(\mathbf{q}_1)\rangle^2\right)\frac{[Q_5(1) - Q_5(2)]^2}{2}$$

$$+\frac{1}{2}\left(\kappa_5 + b_2\langle Q_3^-(\mathbf{q}_1)\rangle^2\right)\frac{[Q_5(1) + Q_5(2)]^2}{2}$$

$$\equiv \frac{1}{2}\kappa_Y Y^2 + \frac{1}{2}\kappa_Z Z^2 \ , \tag{10}$$

where $Y = [Q_5(1) - Q_5(2)]/\sqrt{2}$, and $Z = [Q_5(1) + Q_5(2)]/\sqrt{2}$. This notation (of Table IV) is motivated by the labelling of the axes in the orthorhombic phase (see Eq. (5) and Fig. 3). We therefore see that the presence of a nonzero value of $\langle Q_3^-(\mathbf{q}_1)\rangle$ lifts the degeneracy in energy between the two Q_5^- modes and leads to the proper linear combinations Y and Z as the new normal modes of the Cmcm structure. The analogous splitting occurs in the same way for the Q_5^+ modes and leads to the redefinition of normal modes as $Y^+ = [Q_5^+(1) - Q_5^+(2)]/\sqrt{2}$ and $Z^+ = [Q_5^+(1) + Q_5^+(2)]/\sqrt{2}$.

1. Induced Absorption Modes

We next investigate the mixing of modes due to the nonzero value of $\langle Q_3^-(\mathbf{q}_1)\rangle$. The Hamiltonian we consider for the mixing of absorptive modes is $\mathcal{H}_3 + \mathcal{H}_5 + V_5$, where

$$\mathcal{H}_3 = \frac{1}{2}\kappa_3 \sum_k Q_3^-(\mathbf{q}_k)^2 \ ,$$

$$V_5 = \frac{1}{2}\sum_n\left(\kappa_{U_n}U_n^2 + \kappa_{V_n}V_n^2 + \kappa_{W_n}W_n^2\right)$$

$$+ \sum_n\langle Q_3^-(\mathbf{q}_1)\rangle^n\left(a^{(n)}U_n Z + b^{(n)}V_n Y\right.$$

$$\left. + c^{(n)}W_n Q_3^-(0)\right) \ , \tag{11}$$

where U_n, V_n, W_n are single phonon operators (to be determined) which, as we will see, become optically active by virtue of their coupling to the optically active Z, Y, or $Q_3^-(0)$ modes by the interaction V_5 at order $\langle Q_3^-(\mathbf{q}_1)\rangle^n$. To identify these newly active modes, we analyze the symmetry of the coupling terms in Eq. (11). Note that wave vector conservation indicates that terms in Eq. (11) with n even involve newly active modes at zero wave vector and those with n odd involve newly active zero wave vector modes which, before the

15

distortion, were at wave vector $\mathbf{q}_1$ in the tetragonal Brillouin zone. The character table for the $\mathbf{X}$ wave vectors was given in Table II.

To see more specifically what the Hamiltonian of Eqs. (10) and (11) implies, consider only the terms involving U_n and Z:

$$
\begin{aligned}
\mathcal{H}_X &= \frac{1}{2}\kappa_Z Z^2 + \frac{1}{2}\sum_n \kappa_{U_n} U_n^2 \\
&\quad + \sum_n a^{(n)} \langle Q_3^-(\mathbf{q}_1)\rangle^n U_n Z .
\end{aligned}
\tag{12}
$$

In carrying out perturbation theory relative to the tetragonal phase we use the correct linear combinations Z and Y. At the moment we ignore the perturbation in the energy due to this interaction which was addressed by Eq. (10). Our interest here lies in the mixing of modes. When the quadratic Hamiltonian of Eq. (12) is diagonalized, the new modes $\tilde{U}_n$ perturbed through their coupling to Z will now be

$$
\tilde{U}_n = U_n - \frac{a^{(n)}\langle Q_3^-(\mathbf{q}_1)\rangle^n Z}{\kappa_{U_n} - \kappa_Z} .
\tag{13}
$$

By analogy we will also have new modes

$$
\tilde{V}_n = V_n - \frac{b^{(n)}\langle Q_3^-(\mathbf{q}_1)\rangle^n Y}{\kappa_{V_n} - \kappa_Y}
$$

$$
\tilde{W}_n = W_n - \frac{c^{(n)}\langle Q_3^-(\mathbf{q}_1)\rangle^n Q_3^-(0)}{\kappa_{W_n} - \kappa_3} .
$$

What this means is that the modes U_n, V_n, and W_n (which we will identify in a moment) are optically active because they are linear combinations with the optically active modes Z_k, Y_k, and $Q_3(0)_k$, respectively, whose polarizations they inherit. For quantitative work (see Appendix A), it is necessary to keep track of the coupling to the different optically active modes, Z_k, Y_k, and $Q_3^-(0)_k$. For simplicity, since we are mainly interested in which modes are newly induced, we need not keep the sum over k.

Near $T_>$, $\langle Q_3(\mathbf{q}_1)\rangle$ will be proportional to $(T_> - T)^\beta$, where $\beta = 1/2$ in mean field theory. Thus the temperature dependence of terms with different powers of this variable will be distinguishably different. Analogous terms for the scenario when the wave vector $\mathbf{q}_2$ has condensed can be obtained by applying the operator $\mathcal{R}_4$ to $\mathcal{H}_3 + \mathcal{H}_5 + V_5$. Now we study how symmetry restricts the U's, V's and W's of Eq. (11). Since $\mathcal{R}_4$ is not a relevant symmetry operation, we require $\mathcal{H}_3 + \mathcal{H}_5 + V_5$ to be invariant under $\mathcal{I}$, m_d, and m_z. If n is

16

odd (even), then U_n, V_n, and W_n are at wave vector $\mathbf{q}_1$ (wave vector zero). To be invariant under inversion, U_n, V_n, and W_n have to have parity $(-1)^{n+1}$ under inversion. Also U_n and V_n must be even under $m_z \equiv (xy\bar{z})$ and W_n must be odd under $(xy\bar{z})$. Finally we have to consider the effect of $m_d = (yxz)$. From Tables I and II we find that

$$m_d Y = -Y , \quad m_d Z = Z ,$$

$$m_d Q_3^-(0) = Q_3^-(0) , \quad m_d Q_3^-(\mathbf{q}_1) = -Q_3^-(\mathbf{q}_1) .$$

For V_5 to be invariant under m_d, we therefore must have

$$m_d U_n = (-)^n U_n , \quad m_d V_n = (-)^{n+1} V_n ,$$

$$m_d W_n = (-)^n W_n . \tag{14}$$

Note that all the above constraints depend on n only through $(-1)^n$, so that to find the leading temperature dependences just below $T_>$, we only need to consider two distinct cases, $n = 1$ and $n = 2$. First consider $n = 1$. Then

$$\mathcal{I} U_1(\mathbf{q}_1) = U_1(\mathbf{q}_1) , \quad m_z U_1(\mathbf{q}_1) = U_1(\mathbf{q}_1) ,$$

$$m_d U_1(\mathbf{q}_1) = -U_1(\mathbf{q}_1) , \quad \mathcal{I} V_1(\mathbf{q}_1) = V_1(\mathbf{q}_1) ,$$

$$m_z V_1(\mathbf{q}_1) = V_1(\mathbf{q}_1) , \quad m_d V_1(\mathbf{q}_1) = V_1(\mathbf{q}_1) ,$$

$$\mathcal{I} W_1(\mathbf{q}_1) = W_1(\mathbf{q}_1) , \quad m_z W_1(\mathbf{q}_1) = -W_1(\mathbf{q}_1) ,$$

$$m_d W_1(\mathbf{q}_1) = -W_1(\mathbf{q}_1) ,$$

so that

$$U_1 = \alpha_1 Q_2^+(\mathbf{q}_1) , \quad V_1 = \beta_1 Q_1^+(\mathbf{q}_1) , \quad W_1 = \gamma_1 Q_4^+(\mathbf{q}_1) ,$$

where α_1, β_1, and γ_1 are constants whose values are not fixed by symmetry. The meaning of U_1 is that because of the allowed coupling between Z and *any* operator having the symmetry of $Q_2^+(\mathbf{q}_1)$ this coupling will render all such modes optically active with polarization Z inherited from coupling to Z. This coupling can be analoyzed for each Wykoff orbit, as we do in Table VIII. To summarize: the coupling at first order in $\langle Q_3^-(\mathbf{q}_1) \rangle$, which we denote $V_c^{(1)}$ [and later the superscript 2 indicates second order in $\langle Q_3^-(\mathbf{q}_1) \rangle$] is

$$V_c^{(1)} = \langle Q_3(\mathbf{q}_1) \rangle \left[\sum_{k=1}^{n(X_2^+)]} a_k^{(1)} Z Q_2^+(\mathbf{q}_1)_k \right.$$

17

$$+ \sum_{k=1}^{n(X_1^+)]} b_k^{(1)} Y Q_1^+(\mathbf{q}_1)_k$$

$$+ \sum_{k=1}^{n(X_4^+)]} c_k^{(1)} Q_3^-(0) Q_4^+(\mathbf{q}_1)_k \Bigg] . \tag{15}$$

The fact that there are more than one occurrence of $Q_3(\mathbf{q}_1)$ affects the intensity but not the number or symmetry of new modes, $Q_2^+(\mathbf{q}_1)_k$, $Q_1^+(\mathbf{q}_1)_k$, and $Q_4^+(\mathbf{q}_1)_k$. A more complete treatment of this coupling is given in Appendix A.

We now obtain the $n[\Gamma(\mathbf{q}_1)]$ required in Eq. (15). Using standard methods we find for wave vector $\mathbf{q}_1$ that the reducible representations of the displacement vectors over each orbit have the decomposition

$$\begin{aligned}
\Gamma[a(\mathbf{q}_1)] &= X_2^-(\mathbf{q}_1) + X_3^-(\mathbf{q}_1) + X_4^-(\mathbf{q}_1) , \\
\Gamma[e(\mathbf{q}_1)] &= X_2^-(\mathbf{q}_1) + X_3^-(\mathbf{q}_1) + X_4^-(\mathbf{q}_1) \\
&\quad + X_1^+(\mathbf{q}_1) + X_3^+(\mathbf{q}_1) + X_4^+(\mathbf{q}_1) \\
\Gamma[g(\mathbf{q}_1)] &= 2X_1^-(\mathbf{q}_1) + 2X_2^-(\mathbf{q}_1) + X_3^-(\mathbf{q}_1) \\
&\quad + X_4^-(\mathbf{q}_1) + 2X_1^+(\mathbf{q}_1) + 2X_2^+(\mathbf{q}_1) \\
&\quad + X_3^+(\mathbf{q}_1) + X_4^+(\mathbf{q}_1) ,
\end{aligned} \tag{16}$$

Therefore, for example, $n[X_4^+(\mathbf{q}_1)]$ assumes the values 0, 1, 1 for orbits a, e, and g, respectively, leading to the results in the second column of Table VIII.

We also show figures of the induced absorption modes in Fig. 4. The easiest way to generate a mode of a given symmetry (X_k^+ or X_k^-) is to consider each Wyckoff orbit in turn. For a given orbit assign one site an arbitrary displacement vector (u_x, u_y, u_z), then generate the displacements of the other sites using the characters of Table II. In doing this one will find that one or more of the initial displacements can not be nonzero when one includes the restriction that the wave function have the given wave vector, in this case $\mathbf{q}_1$.

Now we turn to the case $n = 2$, for which

$$\begin{aligned}
\mathcal{I} U_2(0) &= -U_2(0) , \quad m_z U_2(0) = U_2(0) , \\
m_d U_2(0) &= U_2(0) , \quad \mathcal{I} V_2(0) = -V_2(0) , \\
m_z V_2(0) &= V_2(0) , \quad m_d V_2(0) = -V_2(0) , \\
\mathcal{I} W_2(0) &= -W_2(0) , \quad m_z W_2(0) = -W_2(0) , \\
m_d W_2(0) &= W_2(0) .
\end{aligned}$$

TABLE VIII: Number of *additional* optically active modes Q in the orthorhombic Cmcm phase for wave vector $\mathbf{q}_1$. These are given for the Wyckoff orbits a, e, and g, using the decompositions of Eq. (4) for $n[\Gamma_2^-(0)]$ and $n[\Gamma_3^+(0)]$ and of Eq. (16) for $n[X_k^+(\mathbf{q}_1)]$ and $n[X_k^-(\mathbf{q}_1)]$. Pol denotes polarization in the notation of Table V. The order (in the admixture of the wave function) is given as proportional to σ^n, where $\sigma \equiv \langle Q_3^-(\mathbf{q}_1) \rangle$. If the wave function has an admixture of order σ^n, then the cross section has a contribution of order σ^{2n}. TOT refers to the total for 2 a orbits, 3 e orbits and one g orbit. Note that the last row is consistent with the last two rows of Table VII.

	Absorption (Odd parity)				Raman (Even parity)				
Mode	$Q_4^+(\mathbf{q}_1)$	$Q_2^+(\mathbf{q}_1)$	$Q_1^+(\mathbf{q}_1)$	$Q_2^-(0)$	$Q_1^-(\mathbf{q}_1)$	$Q_2^-(\mathbf{q}_1)$	$Q_3^-(\mathbf{q}_1)$	$Q_4^-(\mathbf{q}_1)$	$Q_3^+(0)$
Pol.	X	Z	Y	X	XZ	XY	X^2, Y^2, Z^2	YZ	$Y^2 - Z^2$
Order	σ	σ	σ	σ^2	σ	σ	σ	σ	σ^2
RP(a)	0	0	0	0	0	1	1	1	0
RP(e)	1	0	1	0	0	1	1	1	0
RP(g)	1	2	2	0	2	2	1	1	0
TOT	4	2	5	0	2	7	6	6	0

The solutions for $U_2(0)$ and $V_2(0)$ do not produce new modes but instead add to the intensity of already existing modes. New modes arise from $W_2(0) = Q_2^-(0)$, so that the relevant second order coupling perturbation is

$$V_c^{(2)} = \langle Q_3^-(\mathbf{q}_1) \rangle^2 \sum_{k=1}^{n[\Gamma_2^-(0)]} c_k^{(2)} Q_3^-(0) Q_2^-(0)_k \;,$$

where $n[\Gamma_2^-(0)]$ is given in Eq. (4). We summarize our results in Table VIII. Note that all the newly induced modes have absorption intensity proportional to $\langle Q_3^-(\mathbf{q}_1) \rangle^2$ only because the low symmetry sites of I4/mmm (which allow the OP $Q_2^-(0)$ to appear) are not occupied for CMO or CTO: $n[\Gamma_2^-(0)] = 0$ for CMO or CTO. But an argument equivalent to what we have given here would be needed to establish this result.
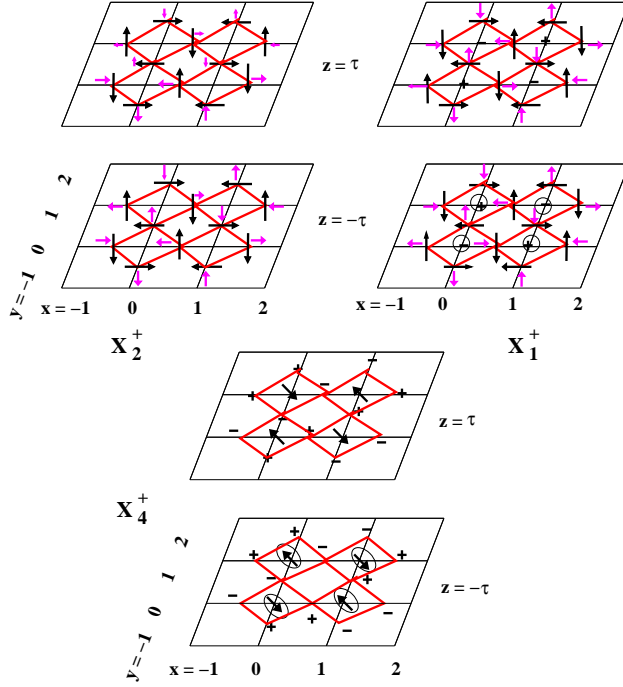
FIG. 4: (Color online) Modes of irrep X_2^+, left and X_1^+, center, and X_4^+, right, all at tetragonal wave vector $\mathbf{q}_1$. These modes become absorption-active in the Cmcm phase. The arrows represent displacements in the x-y plane and $+$ and $-$ are the signs of displacements along the z-axis. Here the thick-lined squares delineate the equatorial oxygens (at $z = \pm\tau$) and the uncircled arrows and $\pm$'s (if any) in the center of the square indicate the displacement of the top apical e-site oxygens in the upper layer of the bilayer at $z = \chi$ and the circled arrows or $\pm$'s (if any) refer to the bottom apical oxygens in the lower layer of the bilayer at $z = -\chi$. All the e-site ions move along the same axis as the apical oxygens, but with independent amplitudes. There are two modes of X_2^+ symmetry corresponding to independently choosing the amplitudes of the large black and small red arrows. If the large black arrow is dominant, this mode is the $(0, 0, \Theta)$ rotation about the tetragonal axis. There are five X_1^+ modes because the displacements of the apical oxygen, the other two e-site ions (not shown), and the two components of the equatorial oxygens are all independent parameters. There are four X_4^+ modes because the tilting, the displacements of the apical oxygens and of the two other e-site ions are independent parameters. (Some of the modes, such as $Q_1^+(\mathbf{q}_1)$ and $Q_4^+(\mathbf{q}_4)$, which grossly distort the octahedra will have relatively high frequencies.) Without the admixtures of order $\langle Q_3^-(\mathbf{q}_1) \rangle$ all these modes are of the wrong symmetry to be optically active. However, the admixing, $e.\ g.$ Eq. (15) in the Cmcm phase makes these modes optically active.

20

Here we consider the admixing of the Raman active modes (see Table I) from irreps Γ_n^+, with $n = 1, 2, 4, 5$:

$$V_C = \sum_n \langle Q_3^-(\mathbf{q_1})\rangle^n \Big[a_n Z^+ T_n + b_n Q_4^+(0)U_n$$
$$+c_n Q_2^+(0)V_n + d_n Q_1^+(0)W_n + e_n Y^+ S_n \Big] ,$$

where T_n, U_n, V_n, W_n, and S_n are the modes which are Raman active by virtue of their coupling proportional to $\langle Q_3^-\rangle(\mathbf{q_1})^n$ to modes of the tetragonal system which are Raman active. For $n = 1$ invariance with respect to $\mathcal{I}$, m_d, and m_z leads to

$$\mathcal{I}S_1(\mathbf{q_1}) = -S_1(\mathbf{q_1}) , \quad m_d S_1(\mathbf{q_1}) = S_1(\mathbf{q_1}) ,$$
$$m_z S_1(\mathbf{q_1}) = -S_1(\mathbf{q_1}) , \quad \mathcal{I}T_1(\mathbf{q_1}) = -T_1(\mathbf{q_1}) ,$$
$$m_d T_1(\mathbf{q_1}) = -T_1(\mathbf{q_1}) , \quad m_z T_1(\mathbf{q_1}) = -T_1(\mathbf{q_1})$$
$$\mathcal{I}U_1(\mathbf{q_1}) = -U_1(\mathbf{q_1}) , \quad m_d U_1(\mathbf{q_1}) = -U_1(\mathbf{q_1}) ,$$
$$m_z U_1(\mathbf{q_1}) = U_1(\mathbf{q_1}) , \quad \mathcal{I}V_1(\mathbf{q_1}) = -V_1(\mathbf{q_1}) ,$$
$$m_d V_1(\mathbf{q_1}) = V_1(\mathbf{q_1}) , \quad m_z V_1(\mathbf{q_1}) = V_1(\mathbf{q_1}) ,$$
$$\mathcal{I}W_1(\mathbf{q_1}) = -W_1(\mathbf{q_1}) , \quad m_d W_1(\mathbf{q_1}) = -W_1(\mathbf{q_1}) ,$$
$$m_z W_1(\mathbf{q_1}) = W_1(\mathbf{q_1}) .$$

So

$$S_1(\mathbf{q_1}) = Q_2^-(\mathbf{q_1}) , \; T_1(\mathbf{q_1}) = Q_1^-(\mathbf{q_1}) , \; U_1(\mathbf{q_1}) = Q_3^-(\mathbf{q_1}) ,$$
$$V_1(\mathbf{q_1}) = Q_4^-(\mathbf{q_1}) , \quad W_1(\mathbf{q_1}) = Q_3^-(\mathbf{q_1}) .$$

Thus

$$V_C^{(n=1)} = \langle Q_3^-(\mathbf{q_1})\rangle \Bigg[\sum_{k=1}^{n(X^-)} a_k^{(1)} Z^+ Q_1^-(\mathbf{q_1})_k$$
$$+ \sum_{k=1}^{n(X_3^-)} b_k^{(1)} Q_4^+(0) Q_3^-(\mathbf{q_1})_k$$
$$+ \sum_{k=1}^{n(X_4^-)} c_k^{(1)} Q_2^+(0) Q_4^-(\mathbf{q_1})_k$$

$$+ \sum_{k=1}^{n(X_3^-)} d_k^{(1)} Q_1^+(0) Q_3^-(\mathbf{q}_1)_k$$

$$+ \left. \sum_{k=1}^{n X_2^-)} e_k^{(1)} Y^+ Q_2^-(\mathbf{q}_1)_k \right] ,$$

where the sums over the number of appearances of the Raman active tetragonal modes is omitted, in analogy with Eq. (15). The fact that $Q_4^+(0)$ and $Q_1^+(0)$ are both coupled to $X_3^-(\mathbf{q}_1)_k$ means that each $X_{3,k}$ mode has two independent admixtures, one, $Q_4^+(0)$, giving a contribution to the Raman tensor $a(\hat{i}\hat{j} + \hat{j}\hat{i}) = a(\hat{K}\hat{K} - \hat{J}\hat{J})$ and the other, $Q_1^+(0)$, giving a contribution to the Raman tensor $b\hat{k}\hat{k} + c(\hat{i}\hat{i} + \hat{j}\hat{j}) = b\hat{I}\hat{I} + c(\hat{J}\hat{J} + \hat{K}\hat{K})$. As a result, the $X_{3,k}^-(\mathbf{q}_1)$ modes have a Raman tensor $b\hat{I}\hat{I} + (c-a)(\hat{J}\hat{J}) + (c+a)\hat{K}\hat{K}$, so that $X_{3,k}^-(\mathbf{q}_1)$ has a Raman polarization we denote (X^2, Y^2, Z^2).

For $n = 2$ invariance with respect to $\mathcal{I}$, m_d, and m_z leads to

$$\begin{aligned}
\mathcal{I} S_2(0) &= S_2(0) , \quad m_d S_2(0) = -S_2(0) , \\
m_z S_2(0) &= -S_2(0) , \quad \mathcal{I} T_2(0) = T_2(0) , \\
m_d T_2(0) &= T_2(0) , \quad m_z T_2(0) = -T_2(0) \\
\mathcal{I} U_2(0) &= U_2(0) , \quad m_d U_2(0) = U_2(0) , \\
m_z U_2(0) &= U_2(0) , \quad \mathcal{I} V_2(0) = V_2(0) , \\
m_d V_2(0) &= -V_2(0) , \quad m_z V_2(0) = V_2(0) , \\
\mathcal{I} W_2(0) &= W_2(0) , \quad m_d W_2(0) = W_2(0) , \\
m_z W_2(0) &= W_2(0) .
\end{aligned}$$

So

$$\begin{aligned}
S_2 &= Y_O^+(0) , \quad T_2 = Z^+ , \\
U_2 &= \alpha Q_1^+(0) + \beta Q_4^+(0) , \\
V_2 &= \alpha' Q_2^+(0) + \beta' Q_3^+(0) , \\
W_2 &= \alpha'' Q_1^+(0) + \beta'' Q_4^+(0) .
\end{aligned}$$

The only new irrep here is $\Gamma_3^+(0)$ with OP $Q_3^+(0)$. So we have the results of Table VIII. As was the case for the absorption cross section, all the newly induced modes have their Raman scattering cross section proportional to $\langle Q_3^-(\mathbf{q}_1) \rangle^2$ only because the low symmetry

sites of I4/mmm (which allow the OP $Q_3^+(0)$ to appear) are not occupied for CMO or CTO. We emphasize that this result is not a general result for the space group I4/mmm distorting into space group Cmcm.

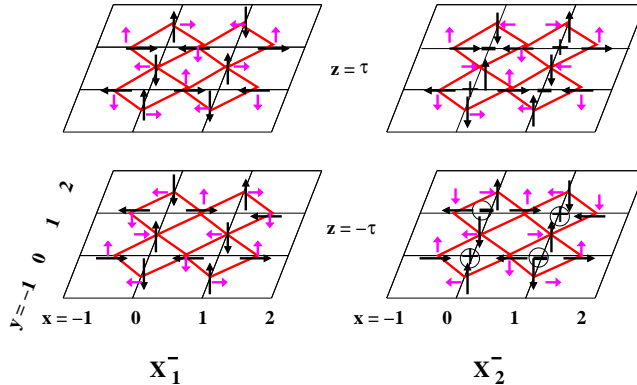In Figs. 5 and 6 we show the new Raman modes in the Cmcm phase.

FIG. 5: (Color online) As Fig. 4 except for modes of irrep X_1^-, left and X_2^-, right, both at tetragonal wave vector $\mathbf{q}_1$. These are the modes which become Raman active (see Table VIII) due to admixtures of tetragonal Raman active zone center modes. In mode X_1^- the sites on the z axis do not move, so there are two modes of this symmetry corresponding to the choice of the amplitudes of the x and y displacements. There are 7 modes of symmetry $X_2^-(\mathbf{q}_1)$ because there are two ways to choose the amplitude of the arrows (the displacements of the equatorial oxygens) and one way to independently choose the amplitudes of the displacements along the z-axis for each of the 2 a orbits and for each of the 3 e orbits of such sites. These breathing modes grossly distort the octahedra and therefore have relatively high frequency.

3. Temperature Dependence of Mode Energies and Absorption Intensities

Near the phase transition at temperature $T = T_>$ where the order parameter $\langle Q_3^-(\mathbf{q}_1)\rangle$ becomes nonzero one has

$$\omega_n(T) = \omega_n^{(0)}(T) + \delta\omega_n(T) \ ,$$
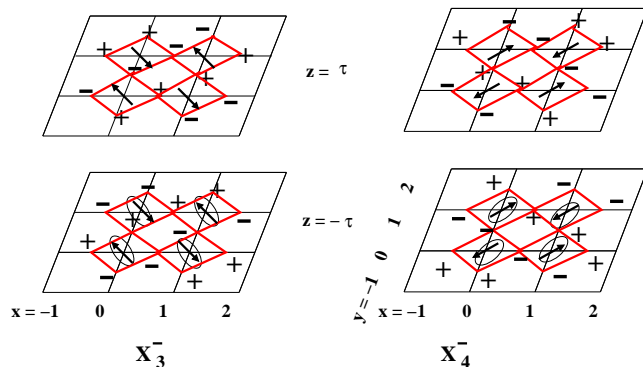$$I_n(T) = I_n^{(0)}(T) + \delta I_n(T) \ , \tag{17}$$

23

FIG. 6: (Color online) As Fig. 5 except for modes of irrep X_3^-, left and X_4^-, right, both at tetragonal wave vector $\mathbf{q}_1$. The equatorial oxygens (g orbits) tilt around the [110] direction for irrep $X_3^-(\mathbf{q}_1)$ and around the [1$\bar{1}$0] direction for $X_4^-(\mathbf{q}_1)$, in each case with a single amplitude. The other ions on the z-axis move along the [1$\bar{1}$0] axis for $X_3^-(\mathbf{q}_1)$ and along the [110] axis for $X_4^-(\mathbf{q}_1)$, in each case with an independent amplitude. Thus for both irreps we have 6 modes (one for each orbit). In the notation of Refs. 29 and 30 $Q_3^-(\mathbf{q}_1)$ is a $(\Phi, \Phi, 0)$ rotation and $Q_4^-(\mathbf{q}_1)$ is a $(\Phi, -\Phi, 0)$ rotation. The wave vector regulates how one bilayer is structured relative to the adjacent bilayer. So these two modes have slightly different frequencies because although their intrabilayer interaction energies are the same, their interbilayer interaction energies are different.

where the first term is the smooth temperature dependence and the second term is the anomalous term at the phase transition which is only nonzero for $T < T_>$ and will involve powers of $\langle Q_3^-(\mathbf{q}_1) \rangle \equiv \sigma \sim |T_> - T|^\beta$, where the order parameter exponent β is $1/2$ in mean field theory, but fluctuations will cause it to be less than $1/2$.

First consider the mode energies. For all the *nondegenerate* $\mathbf{q} = 0$ modes, the perturbation of the form given in Eq. (11), will lead to an energy shift from terms with $n = 1$, which, in second order perturbation theory, gives a contribution to $\delta\omega(T)$ of order $\sigma^2 \sim |T_> - T|^{2\beta}$. For the *degenerate* $\Gamma_5^\pm(0)$ modes, $\delta\omega(T)$ has a contribution from first order perturbation theory, but in that case, since b_1 of Eq. (9) vanishes, the contribution to $\delta\omega(T)$ is again of order $\sigma^2 \sim |T_> - T|^{2\beta}$. These results are shown in the left-hand panels of Fig. 7. It should also be noted that the mode energies can be modified by quartic terms in the Hamiltonian which we have not so far considered and which are of the form[34,35]

$$V_4 = \sum_n d_n U_n^2 Q_3^-(\mathbf{q}_1)^2$$

24

which will also lead to a contribution to $\delta\omega(T)$ of order $\sigma^2 \sim |T_> - T|^{2\beta}$. It is plausible, but not a certainty, that the sign of the anomalous contribution would cause a stiffening of the modes as the temperature is reduced as is depicted in lower left-hand panel of Fig. 7. If V_4 were to be neglected, then one would have a direct correlation between $\delta I_n(T)$ and $\delta\omega_n(T)$.[36]

Now consider the mode intensities in the presence of admixtures written in Eq. (13). The standard scenario in perturbation theory is that a perturbation in first order introduces new components into the wave function without changing the unperturbed component of the wave function. In second order perturbation theory the amplitude of the unperturbed component of the wave function can be modified. Here, this tells us that if the mode U_n is already dipole allowed, then the intensity will be modified at order σ^2. If the mode U_n is not allowed in the absence of the perturbation then its intensity will be proportional to the square of the amplitude of the admixture. Furthermore, new modes that appear at first order in σ will have intensity of the form of Eq. (17) with $I_n^{(0)}(T) = 0$ and $\delta I(T) \sim \sigma^2 \sim |T_> - T|^{2\beta}$. New modes that only appear at second order in σ will have intensity of the form of Eq. (17) with $I_n^{(0)}(T) = 0$ and $\delta I(T) \sim \sigma^4 \sim |T_> - T|^{4\beta}$. From Table VIII we see that for CMO or CTO there are no such modes that only appear at order σ^2. This is a special property of the RP system. Had we had a more general tetragonal system with low symmetry sites, then there would be modes which only appear at order σ^2 and which would have $\delta I(T) \sim \sigma^4 \sim |T_> - T|^{4\beta}$. Our results are summarized in the right-hand panels of Fig. 7.

IV.   CMC2$_1$ PHASE

A.   Analysis based on Cmc2$_1$ symmetry

Since Cmc2$_1$ does not have a center of inversion symmetry, parity is not a good quantum number and Raman and absorption modes are mixed. In Cmc2$_1$ the general orbit is half as large as for Cmcm. However, the unit cell then contains twice as many orbits. The sites in Cmc2$_1$ are given in Table IX and the character table for $\mathbf{q} = 0$ is given in Table X.

Using the data in Table X we find that

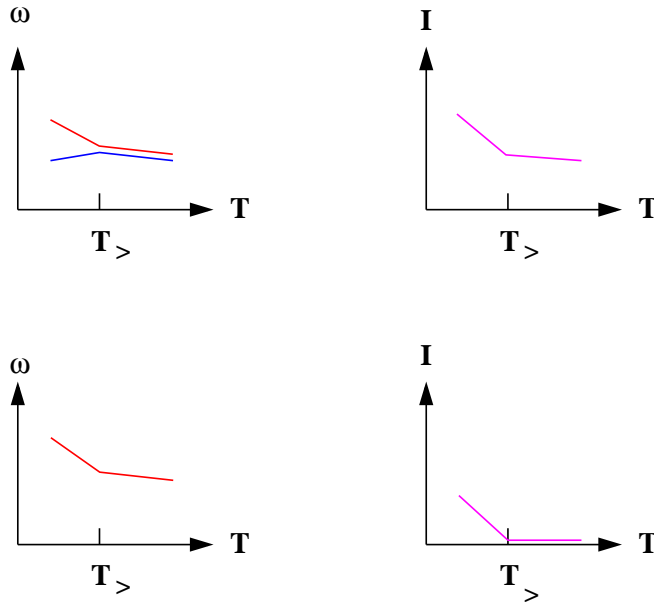$$\Gamma(a_{Cmc2_1}) = 2\Gamma_1 + 2\Gamma_2 + \Gamma_3 + \Gamma_4 \,,$$

FIG. 7: (Color online) RP modes. Left panels: mode energy versus temperature, where $T_>$ is the temperature at which $\langle Q_3^-(\mathbf{q}_1)\rangle$ becomes nonzero. Right panels: the mode intensity versus temperature. Upper left: removal of degeneracy of the $\Gamma_5^{\pm}$ modes. Lower left: temperature dependence of a nondegenerate mode energy. Upper right: temperature dependence of the intensity of a nondegenerate mode which is absorption allowed in the tetragonal phase. Lower right: temperature dependence of nondegenerate mode intensity for modes which have zero intensity in the tetragonal phase. In all cases, the discontinuity in slope is drawn assuming the mean-field result, $\beta = 1/2$, for the order parameter exponent. Otherwise, the lower temperature additional contribution is of order $|T_> - T|^{2\beta}$.

TABLE IX: Operators for $Cmc2_1$.

$$
\begin{array}{ll}
E = (x, y, z) & 2_z = (\overline{x}, \overline{y}, 1/2 + z) \\
m_x = (\overline{x}, y, z) & m_y = (x, \overline{y}, 1/2 + z)
\end{array}
$$

$$
\Gamma(e_{Cmc2_1}) \;=\; 3 \sum_{n=1}^{4} \Gamma_n \;,\;\; \Gamma(g_{Cmc2_1}) = 6 \sum_{n=1}^{4} \Gamma_n \;, \tag{18}
$$

and the dipole moments and Raman tensors of each irrep are given in Table X. Note that once we have identified the absorption modes, the identification of the Raman active modes follows, except for those of irrep Γ_3. Using Eq. (18) we find the number of optically active

26

TABLE X: Character table for the little group at $\mathbf{q} = 0$ for the Cmc2$_1$ lattice. The last three columns are the characters for the various tetragonal orbits on the Cmc2$_1$ structure. Orthorhombic coordinates are used throughout this table. $\mathbf{P}$ gives the nonzero component of the dipole moment operators for the irrep in question. The Raman tensors $\mathbf{R}$ are $\mathbf{R}(\Gamma_1) = d\hat{I}\hat{I} + e\hat{J}\hat{J} + f\hat{K}\hat{K}$, $\mathbf{R}(\Gamma_2) = g(\hat{J}\hat{K} + \hat{K}\hat{J})$, $\mathbf{R}(\Gamma_3) = h(\hat{I}\hat{J} + \hat{J}\hat{I})$, and $\mathbf{R}(\Gamma_4) = i(\hat{I}\hat{K} + \hat{K}\hat{I})$.

Operator	Γ_1	Γ_2	Γ_3	Γ_4	a	e	g
(X, Y, Z)	1	1	1	1	6	12	24
$(\overline{X}, Y, Z)$	1	1	-1	-1	2	0	0
$(\overline{X}, \overline{Y}, 1/2 + Z)$	1	-1	1	-1	0	0	0
$(X, \overline{Y}, 1/2 + Z)$	1	-1	-1	1	0	0	0
$\mathbf{P}$	$a\hat{K}$	$b\hat{J}$	None	$c\hat{I}$			

modes in the Cmc2$_1$ phase given in Table XI.

B. Analysis based on lowering of Cmcm symmetry

Now we perform the analysis of mode symmetry using the mixing of modes in terms of the OP's present in the Cmc2$_1$ phase, namely $Q_3^-(\mathbf{q}_1)$, $Z \equiv [\Gamma_{5,1}^- + \Gamma_{5,2}^-]/\sqrt{2}$, and $Q_2^+(\mathbf{q}_1)$, where we assume the OP's of the family of $\mathbf{q}_1$. (Afterwards the analogous terms associated with $\mathbf{q}_2$ can be obtained by applying the four-fold rotation $\mathcal{R}_4$ to the coupling we construct for $\mathbf{q}_1$.) At the lower transition we can mix using all the condensed order parameters, $Q_3^-(\mathbf{q}_1)$, $Q_2^+(\mathbf{q}_1)$, and Z. The first question is: can we induce $Y \equiv Q_{5,1}^-(0) - Q_{5,2}^-(0)$? The answer is no. Note that $\boldsymbol{\sigma}_d Z = Z$ and $\boldsymbol{\sigma}_d Y = -Y$. Also $\boldsymbol{\sigma}_d Q_3^-(\mathbf{q}_1) = -\boldsymbol{\sigma}_d Q_3^-(\mathbf{q}_1)$ and $\boldsymbol{\sigma}_d Q_2^+(\mathbf{q}_1) = -Q_2^+(\mathbf{q}_1)$. But for wave vector conservation we must have a total even number of powers of these two operators at $\mathbf{q}_1$. Hence there can be no term in the free energy which is linear in Y. So Y is not induced by the other order parameters.

TABLE XI: As Table X. Optically active modes of the Cmc2$_1$ phase. TOT gives the total number of modes of each symmetry found using Eq. (18) and Table X. We copy the number of modes in the Cmcm phase from Table VII and Addl gives the number of new modes which appear when the Cmc2$_1$ phase is reached, as given in Eqs. (20) and (24). Here R refers to Raman active modes and P to dipole-active modes. This entry includes only the additional modes we explicitly calculated for the dipole active modes and for the Raman active modes which are *not* dipole active. Since the total number of modes is given for both Cmcm and Cmc2$_1$, one can deduce that, for instance, the number of additional Raman active modes with Raman tensor $i(\hat{I}\hat{K} + \hat{K}\hat{I})$ is 17-7=10.

Irrep	Γ_1	Γ_2	Γ_3	Γ_4
P	$a\hat{K}$	$b\hat{J}$	None	$c\hat{I}$
TOT	19	19	17	17
Cmcm	10(R), 9(P)	7(R), 12(P)	12(R)	7(R), 10(P)
Addl	10(P)	7(P)	5(R)	7(P)

1. Induced Absorption Modes

So optically active absorption modes are admixed by the perturbation

$$V(\mathbf{q}_1) = \sum_{k,l,m} \langle Q_3^-(\mathbf{q}_1)\rangle^k \langle Q_2^+(\mathbf{q}_1)\rangle^l \langle Z\rangle^m$$

$$\times \left(a_{klm}U_{klm}Z + b_{klm}V_{klm}Y + c_{klm}W_{klm}Q_3^-(0) \right),$$

where again the U's, V's, and W's are the single phonon operators which will become optically active due to this mechanism and which we wish to identify. We insert the angle brackets to emphasize that these higher order terms give rise to an effective bilinear coupling of the type that mixes modes. In principle any perturbation has to be invariant under all the symmetries of the tetragonal phase. However, applying a four-fold rotation takes $\mathbf{q}_1$ into $\mathbf{q}_2$ (whose order parameters are zero) and $\langle Z\rangle$ into $\langle Y\rangle$ (which is also zero). Thus we require that $V(\mathbf{q}_1)$ be invariant under only m_d, m_z, and $\mathcal{I}$, in which case

$$m_d U_{klm} = (-)^{k+l+1}U_{klm}, \quad m_d V_{klm} = (-)^{k+l}V_{klm},$$

$$m_d W_{klm} = (-)^{k+l+1}W_{klm}, \quad m_z U_{klm} = U_{klm},$$

$$m_z V_{klm} = V_{klm}, \quad m_z W_{klm} = -W_{klm}$$

28

$$\mathcal{I}U_{klm} = (-)^{k+m+1}U_{klm} , \quad \mathcal{I}V_{klm} = (-)^{k+m+1}V_{klm} ,$$

$$\mathcal{I}W_{klm} = (-)^{k+m+1}W_{klm} .$$

TABLE XII: Independent sets of indices for the operators U, V, or W (which depend on $(-)^{k+m}$ and $(-)^{k+l}$). "Cmcm" indicates equality to cases previously considered for Cmcm. The equal sign indicates equality in view of $\langle Z \rangle \propto \langle Q_3^-(\mathbf{q}_1) \rangle \langle Q_2^+(\mathbf{q}_1) \rangle$. Cases which lead to identical operators with different prefactors are indicated by "$\propto$." Cases which produce "new" operators are indicated by $*$.

$k =$	0	0	1	1	1	0	1
$l =$	0	1	0	1	0	1	1
$m =$	1	0	0	0	1	1	1
Case	A	B	C	D	E	F	G
New?	$*$	$*$	Cmcm	$=$A	$\propto$ B	$=$C	$\propto$ C

We use the result of Ref. 9 that, due to the cubic coupling between the order parameters, one has

$$\langle Z \rangle = a \langle Q_2^+(\mathbf{q}_1) \rangle \langle Q_3^-(\mathbf{q}_1) \rangle , \tag{19}$$

where a is a constant. Note the following: a) increasing k, l, or m by two does not induce an additional operator and b) solutions for U, V, and W, depend on $k+l$ and $k+m$. Therefore we have the results of Table XII of which we only consider cases A, B, and E. We find that

$$U_{001} = cQ_1^+(0) + dQ_4^+(0) , \quad V_{001} = c'Q_2^+(0) + d'Q_3^+(0) ,$$

$$W_{001} = Z^+ , \quad U_{101} = U_{010} = Q_3^-(\mathbf{q}_1) ,$$

$$V_{101} = V_{010} = Q_4^-(\mathbf{q}_1) , \quad W_{101} = W_{010} = Q_1^-(\mathbf{q}_1) . \tag{20}$$

From these three cases we get (for wave vector $\mathbf{q}_1$)

$$V(\mathbf{q}_1) = \langle Q_2^+(\mathbf{q}_1) \rangle \langle Q_3^-(\mathbf{q}_1) \rangle \Big\{ a_1 Q_3^-(0)Z^+ + Z[$$

$$a_2 Q_1^+(0) + a_3 Q_4^+(0)] + Y[a_4 Q_2^+(0) + a_5 Q_3^+(0)] \Big\}$$

29

$$+\langle Q_2^+(\mathbf{q}_1)\rangle \Big\{ a_6 Z Q_3^-(\mathbf{q}_1) + a_7 Y Q_4^-(\mathbf{q}_1)$$

$$+a_8 Q_3^-(0) Q_1^-(\mathbf{q}_1) \Big\} + \langle Q_2^+(\mathbf{q}_1)\rangle \langle Q_3^-(\mathbf{q}_1)\rangle^2 \Big\{$$

$$a_9 Z Q_3^-(\mathbf{q}_1) + a_{10} Y Q_4^-(\mathbf{q}_1) + a_{11} Q_3^-(0) Q_1^-(\mathbf{q}_1) \Big\} .$$

$$\tag{21}$$

By applying $\mathcal{R}_4$ to this we get

$$V(\mathbf{q}_2) = \langle Q_2^+(\mathbf{q}_2)\rangle \langle Q_3^-(\mathbf{q}_2)\rangle \Big\{ a_1 Q_3^-(0) Y^+ + Y[$$

$$a_2 Q_1^+(0) - a_3 Q_4^+(0)] + Z[a_4 Q_2^+(0) - a_5 Q_3^+(0)] \Big\}$$

$$+\langle Q_2^+(\mathbf{q}_2)\rangle \Big\{ a_6 Y Q_3^-(\mathbf{q}_2) + a_7 Z Q_4^-(\mathbf{q}_2)$$

$$+a_8 Q_3^-(0) Q_1^-(\mathbf{q}_2) \Big\} + \langle Q_2^+(\mathbf{q}_2)\rangle \langle Q_3^-(\mathbf{q}_2)\rangle^2 \Big\{$$

$$a_9 Y Q_3^-(\mathbf{q}_2) + a_{10} Z Q_4^-(\mathbf{q}_2) + a_{11} Q_3^-(0) Q_1^-(\mathbf{q}_2) \Big\} .$$

$$\tag{22}$$

2. Induced Raman Modes

Finally, we carry out the same analysis to determine the new Raman modes of polarization $X_O Y_O$, since these modes are not dipole active and hence are not accessible to the previous calculation. To get polarization $X_O Y_O = z_t(x_t - y_t)$ we must induce the mode Y^+ of irrep Γ_5^+. We use the results of Table XII to restrict our attention to the coupling for the cases $k = l = m - 1 = 0$ (together with $k = l = m + 1 = 1$) and $k = l - 1 = m = 0$ (together with $k = l + 1 = m = 1$) so that

$$V = R_1 Y^+[\alpha\langle Z\rangle + \beta\langle Q_2^+(\mathbf{q}_1)\rangle \langle Q_3^-(\mathbf{q}_1)\rangle]$$

$$+R_2 Y^+[\gamma\langle Q_2^+(\mathbf{q}_1)\rangle + \delta\langle Q_3^-(\mathbf{q}_1)\rangle \langle Z\rangle] ,$$

$$\tag{23}$$

where R_k are the single phonon operators which we determine by requiring that V be an invariant under $\mathcal{I}$, m_d, and m_z. we find that

$$R_1 = Q_1(0) \text{ or } Q_4^-(0) , \quad R_2 = Q_3^+(\mathbf{q}_1) . \tag{24}$$

TABLE XIII: *Additional* optically active modes (which we refer to as 'new') which appear in the $Cmc2_1$ phase for wave vector $\mathbf{q}_1$ from Eqs. (20) and (24). The values of $n[(\Gamma(0)]$ for each orbit are given in Eq. (3) and those of $n[(\Gamma(\mathbf{q})]$ are given in Eq. (16). TOT is the total number of modes from 2a orbits, 3e orbits, and one g orbit. The values of $\mathbf{P}$ (and the associated values of the Raman tensor $\mathbf{R}$) are from Z, Y and $Q_3^-(0)$ in Eq. (21). The values of the Raman tensor $\mathbf{R}$ for $Q_4^-(0)$ is inherited from Y^+ in Eq. (23). In the last row the entry 1 indicates that the Raman tensor is $\mathcal{R} = a\hat{I}\hat{I} + b\hat{J}\hat{J} + c\hat{K}\hat{K}$.

	New zero wave vector modes							New modes for wave vector $\mathbf{q}_1$			
Orbit	$Q_1^+(0)$	$Q_4^+(0)$	$Q_2^+(0)$	$Q_3^+(0)$	Z^+	$Q_1^-(0)$	$Q_4^-(0)$	$Q_3^-(\mathbf{q}_1)$	$Q_4^-(\mathbf{q}_1)$	$Q_1^-(\mathbf{q}_1)$	$Q_3^+(\mathbf{q}_1)$
a	0	0	0	0	0	0	0	1	1	0	0
e	1	0	0	0	1	0	0	1	1	0	1
g	1	0	1	0	2	0	1	1	1	2	1
TOT	4	0	1	0	5	0	1	6	6	2	4
$\mathbf{P}$	Z	Z	Y	Y	X	none	none	Z	Y	X	none
$\mathbf{R}$	1	1	YZ	YZ	XZ	none	XY	1	YZ	XZ	XY

The number of modes we admix into R_1 is equal to the number of times either $\Gamma_1^-(0)$ or $\Gamma_4^-(0)$ appears, which from Eq. (3) is one for each g orbit or once in all. The number of modes we admix into R_2 is equal to the number of times irrep $\Gamma_3^+(\mathbf{q}_1)$ appears, which from Eq. (16) is one for each e orbit and one for each g orbit, or four in all. So there are five additional $X_O Y_O$ Raman modes induced in $Cmc2_1$.

We could give figures showing the displacements in the new optically active modes which appear in the $Cmc2_1$ phase. Actually, the new modes at wave vector $\mathbf{q}_1$ have already been shown in Figs. 4, 5, and 6, but now many of these modes are both absorption active and Raman active. We leave it to the reader to draw the new modes at zero wave vector using the same technique as used above.

3. Summary of Optically Active Phonons.

In Table XIV we list the irreps of the tetragonal phase which are active or become active due to the condensation of order parameters $Q_3^-(\mathbf{q})$, $Q_2^+(\mathbf{q})$, and $\Gamma_5^-(0)$. However, one can show that the intensities for wave vector $\mathbf{q}_2$ are obtained from those for wave vector $\mathbf{q}_1$ by simply replacing $\mathbf{q}_1$ by $\mathbf{q}_2$.

TABLE XIV: The irrep labels are according to the tetragonal structure. "Pol" denotes polarization, where capitals (lower case) refers to orthorhombic (tetragonal) coordinates, "Int" denotes intensity, and "Modes" denotes the number of modes. The columns labeled $\mathbf{q}_n$ apply when the wave vector $\mathbf{q}_n$ is selected. $\sigma_1 = \sum_l \beta_{kl} \langle Q_{3,l}^-(\mathbf{q}) \rangle^2$, $\sigma_2 = \sum_{l,m} \gamma_{klm} \langle Q_{3,l}^-(\mathbf{q}) \rangle^2 \langle Q_{2,m}^+(\mathbf{q}) \rangle^2$, and $\sigma_{3,k} = \sum_{lm} \langle Q_{2,l}^+(\mathbf{q}) \rangle^2 \gamma_{klm} + \delta_{klm} \langle Q_{3l}^-(\mathbf{q}) \rangle^2]^2$, where k is the mode index and α, β, and γ do not depend on the OP's.

Phase	Irrep	Int	Modes	Pol	
				x	
I4/mmm	Γ_5^- α_k		7	x	
	Γ_5^- α_k		7	y	
	Γ_5^- α_k		6	z	
				$\mathbf{q}_1$	$\mathbf{q}_2$
Cmcm	X_1^+	σ_{1k}	5	Y	Z
	X_2^+	σ_{1k}	2	Z	Y
	X_4^+	σ_{1k}	4	X	X
Cmc2$_1$	Γ_1^+	σ_{2k}	4	Z	Y
	Γ_2^+	σ_{2k}	1	Y	Z
	Γ_5^+	σ_{2k}	5	X	X
Cmc2$_1$	X_3^-	σ_{3k}	6	Z	Y
	X_4^-	σ_{3k}	6	Y	Z
	X_1^-	σ_{3k}	2	X	X

V. MAGNETOELASTIC MODES

Here we investigate the mixing of dipole active phonons with magnons for the RP system containing the magnetic ion Mn^{4+}. The motivation for this investigation is that photon absorption by magnons normally proceeds via a magnetic dipole matrix element, whereas absorption by phonons proceeds via the very much larger electric dipole matrix element. In magnetic ferroelectrics, magnons into which phonons are mixed have been dubbed "electromagnons."[20] Such magnons not only have a much enhanced absorption cross section, but, because their energy is often much lower than the phonon energies, they can also lead to large anomalies in the static dielectric constant.[23] Potentially the same effect is possible here if the magnons have a nontrivial coupling to phonons.

To start we review what is known about the magnetic structure of CMO which appears below the magnetic ordering temperature of 115K.[37] The OP's are[37] $G_X(\mathbf{q_1})$, $C_Y(\mathbf{q_1})$, and F_Z, or equivalently [9] $G_X(\mathbf{q_2})$, F_Y, and $C_Z(\mathbf{q_2})$, where G, F and C are the Wollan-Koehler magnetic structural descriptors[38] for the magnetism of a single bilayer: F denotes a ferromagnetic structure, G and C are the antiferromagnetic structures illustrated in Fig. 8. The wave vector distinguishes between the two possible stacking (of G and C) as one goes from one bilayer to the next,[9] as shown in Fig. 8. As mentioned below Eq. (1) one can select the wave vector by cooling through $T_>$ in the presence of a shear stress.
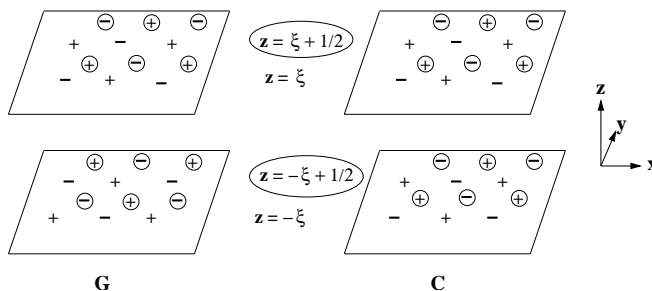

FIG. 8: Spin states of a bilayer of Mn ions at $z = \pm\xi$. The plus and minus signs represent the signs of any component of spin. Left: the "G" configuration. Right the "C" configuration. The uncircled symbols are in the planes at $z = \pm\xi$ and the circled symbols represent the spins in planes at $z = 1/2\pm\xi$ when $\mathbf{q} = \mathbf{q_1}$. For $\mathbf{q} = \mathbf{q_2}$ the circled $+$ and $-$ signs are interchanged. The tetragonal axes are shown at right.

The plan of our analysis is as follows. We will construct the most general trilinear

coupling which involves two magnetic OP's (in order to satisfy time-reversal invariance) and one phonon operator whose wave vector is either at the zone center or at an X point. We will require invariance with respect to all the symmetries of the tetragonal lattice. (As a short-cut we fix the wave vector to be $\mathbf{q}_1$. The terms involving $\mathbf{q}_2$ can be determined later by applying a four-fold rotation to those we find for $\mathbf{q}_1$.) We then develop an effective bilinear coupling by replacing one of the magnetic OP's by its value at the minimum of the free energy.

Thus we analyze in detail the cubic interaction (involving the wave vector $\mathbf{q}_1$)

$$
\begin{aligned}
V_{\mathrm{ME}}(\mathbf{q}_1) &= \sum_{\alpha\beta\gamma}[A_{\alpha\beta\gamma}C_\alpha(\mathbf{q}_1)M_\beta Q_\gamma^+(\mathbf{q}_1) \\
&\quad + B_{\alpha\beta\gamma}C_\alpha(\mathbf{q}_1)N_\beta(\mathbf{q}_1)Q_\gamma^-(0) \\
&\quad + C_{\alpha\beta\gamma}M_\alpha N_\beta(\mathbf{q}_1)Q_\gamma^-(\mathbf{q}_1)] \\
&\equiv \sum_{k=1}^{3} V_{\mathrm{ME}}^{(k)}(\mathbf{q}_1) ,
\end{aligned}
\tag{25}
$$

where $\mathbf{M}$ denotes $\mathbf{F}$, $\mathbf{N}(\mathbf{q})$ denotes $\mathbf{G}(\mathbf{q})$, and we chose the arguments of the phonon operators so as to conserve wave vector. We also used the transformation properties of the magnetic OP's under inversion (see Table XV) to infer the inversion signature of the Q's in Eq. (25).

TABLE XV: The symmetry for components X, Y, and Z of the magnetic OP's (which are pseudovectors). Here $S_X = S_z$, $S_Y = S_x - S_y$, $S_Z = S_x + S_y$, where capitals refer to orthorhombic and lower case to tetragonal coordinates. The results do not depend on the choice of wave vector. In the text we use the standard notation in which the net magnetization, here $\mathbf{F}$, is denoted $\mathbf{M}$ and the staggered magnetization, here $\mathbf{G}(\mathbf{q})$, is denoted $\mathbf{N}(\mathbf{q})$.

Structure	$\mathbf{q}$	$\mathcal{I}$			m_z			m_d		
		Z	Y	X	Z	Y	X	Z	Y	X
F	0	$+$	$+$	$+$	$-$	$-$	$+$	$-$	$+$	$-$
G	$\mathbf{q}$	$-$	$-$	$-$	$+$	$+$	$-$	$-$	$+$	$-$
C	$\mathbf{q}$	$+$	$+$	$+$	$-$	$-$	$+$	$-$	$+$	$-$

To get the effective coupling between magnons and phonons we only analyze special terms of Eq. (25). We take the expectation value (that minimizes the free energy) of one of the

TABLE XVI: The symmetry of the magnetoeleastic trilinear interaction for wave vector $\mathbf{q}_1$. All components are with respect to orthorhombic coordinates. The variables C and N are at wave vector $\mathbf{q}_1$, as are the irreps X_k. Under m_d (m_z) we give the effect of m_d (m_z) on each of the two magnetic OP's. Then the irrep(s) is identified so as to make the trilinear interaction invariant under m_d and m_z and in the next-to-last column we identify the polarization P of the absorption mode (if any). Only irreps that are optically active are included in the analysis. In the last column we give the order of magnitude of the term, assuming the staggered moment to be unity.

Interaction	m_d	m_z	irrep	P	Int.
$M_Z\ N_Y\ Q^-(\mathbf{q}_1)$	$-\ +$	$-\ +$	X_1^-	X	$M^2\langle Q_2^+(\mathbf{q}_1)\rangle^2$
$M_Y\ N_X\ Q^-(\mathbf{q}_1)$	$+\ -$	$-\ -$	X_3^-	Z	$M^2\langle Q_2^+(\mathbf{q}_1)\rangle^2$
$C_X\ N_X\ Q^-(0)$	$-\ -$	$+\ -$	Γ_3^-	X	C^2
$C_Z\ N_X\ Q^-(0)$	$-\ -$	$-\ -$	Γ_5^-	Z	C^2
$C_Y\ N_Y\ Q^-(0)$	$+\ +$	$-\ +$	Γ_3^-	X	C^2
$M_X\ C_Y\ Q^+(\mathbf{q}_1)$	$-\ +$	$+\ -$	X_4^+	X	$C^2M^2\langle Q_3^-(\mathbf{q}_1)\rangle^2$
$M_Y\ C_Y\ Q^+(\mathbf{q}_1)$	$+\ +$	$-\ -$	X_1^+	Y	$C^2M^2\langle Q_3^-(\mathbf{q}_1)\rangle^2$
$M_Z\ C_Z\ Q^+(\mathbf{q}_1)$	$-\ -$	$-\ -$	X_1^+	Y	$C^2M^2\langle Q_3^-(\mathbf{q}_1)\rangle^2$

magnetic OP's and therefore arrive at a quadratic interaction between the other (active) magnetic OP and a phonon OP. To get a magnon-phonon coupling out of this we select the component of the active magnetic OP to be *transverse* to its equilibrium value. Since the nonzero equilibrium component of $\mathbf{N}(\mathbf{q}_1)$ is its X component, the transverse components of $\mathbf{N}(\mathbf{q}_1)$ are its Y and Z components. These are the components of $\mathbf{N}(\mathbf{q}_1)$ which, in the Holstein-Primakoff formulation, create spin waves. The operator Q creates or destroys a phonon. These terms which mix magnons and phonons give rise to "electromagnons."[20–23] We treat the other trilinear terms similarly, keeping only those in which one magnetic OP is longitudinal and the other magnetic OP is transverse. Thereby we have the cases listed in Table XVI for wave vector $\mathbf{q}_1$. The results for wave vector $\mathbf{q}_2$ are quite similar: the polarizations Y and Z are interchanged and in the intensities $\mathbf{q}_1$ is replaced by $\mathbf{q}_2$, as in Table XIV. It is relevant to try to estimate which of these terms are the most significant. For that purpose we keep in mind the fact that the OP's $\mathbf{M}$ and $\mathbf{C}(\mathbf{q}_1)$ are roughly one tenth

as large as $\mathbf{N}(\mathbf{q}_1)$.[37] In addition the optical activity of the phonon depends on whether it is allowed in the tetragonal phase or depends, for its activity, on the distortions of irreps X_3^- or X_2^+ (in this connection we ignore Γ_5^-). It seems likely, then, that the largest magnon-phonon coupling will involve coupling the transverse moment of $C(\mathbf{q}_1)$ to either X or Z polarized zone center phonons. But for completeness, we list the other possibilities. Table XVI only gives results for the case when wave vector $\mathbf{q}_1$ is selected. Results for wave vector $\mathbf{q}_2$ can be obtained by replacing Z polarization by Y and $\mathbf{q}_1$ by $\mathbf{q}_2$, as is done in Table XIV.

These couplings can be detected either by anomalies in the static dielectric constant when magnetic order appears,[23] or by anomalous electric dipole intensity in magnons due to their coupling with optical phonons.[20–22,24]

VI. CONCLUSIONS

In this paper the effect on the optical properties of zone center phonons of the sequential lowering of symmetry by structural distortions from the high symmetry tetragonal (I4/mmm) phase has been studied. In addition, the coupling of the magnons which appear at low temperatures in the magnetically order phase of $Ca_3Mn_2O_7$ and the phonons is explored to identify possible giant enhancements in the magnon cross section in the electromagnetic spectrum.

Our specific results include

•1. We have tabulated the zone center phonon modes with their polarizations which appear in the absorption spectrum and in the Raman scattering spectrum of the I4/mmm, Cmcm, and Cmc2$_1$ phases for $Ca_3X_2O_7$ systems, where X is Mn or Ti.

•2. For modes which become optically active by virtue of a structural distortion, we indicate the dependence of their cross sections on the newly emerging order parameters near the phase boundary where the structural symmetry is lowered. We also discuss the anomalies in the phonon frequencies as the phase boundaries are crossed.

•3. We discuss the symmetry of the magnon phonon interaction which can lead magnons being electric dipole active and hence having anomalously large absorption cross section and leading to analogous large magnetic contributions to the dielectric constant.

Appendix A: Intensity Calculation

1. Tetragonal Phase

In this appendix I discuss in detail how the intensities of the modes are calculated assuming the perturbative description relative to the tetragonal phase is justified. In the tetragonal phase we have the optically active phonons of irreps Γ_5^- and Γ_3^-, governed by the Hamiltonian

$$\mathcal{H}_{\mathrm{TET}} = \frac{1}{2}\sum_{k=1}^{n(\Gamma_5^-)}\kappa_{\perp,k}(Y_k^2 + Z_k^2) + \frac{1}{2}\sum_{k=1}^{n(\Gamma_3^-)}\kappa_{\|,k}X_k^2 ,$$

where it is conveneient to work in orthorhombic coordinates, so that modes X, Y, and Z are polarized along these respective orthorhombic direction. $X_k = Q_3^-(0)_k$, $Y_k = (Q_5^-(1)_k - Q_5^-(2)_k)/\sqrt{2}$, and $Z_k = (Q_5^-(1)_k + Q_5^-(2)_k)/\sqrt{2}$ are the order parameters for the modes of the optically active Γ_3^- and Γ_5^- irreps. To be specific: we number the modes in order of incresing energy.

The coupling to photons is via the dipole moment operator which we write as

$$\mathbf{p} = \sum_{k=1}^{n(\Gamma_5^-)}p_{\perp,k}[Y_k\hat{Y} + Z_k\hat{Z}] + \sum_{k=1}^{n(\Gamma_3^-)}p_{\|,k}X_k\hat{X} ,$$

where $\hat{X}$ is a unit vector in the orthorhombic X direction and similarly for $\hat{Y}$ and $\hat{Z}$. So the absorption intensity in the tetragonal phase of the kth doubly degenerate Y_k-Z_k mode is $Ap_{\perp,k}^2$ and that of the kth X mode is $Ap_{\|,k}^2$, where here and below we set $A = 1$. Since the dipole moment matrix elements are subject to a first principles calculation, it makes sense to give explicit results in terms of calculable quantities.

2. Cmcm Phase

The Hamiltonian that describes the mixing of new optically active phonons in the Cmcm phase is

$$\mathcal{H}_{\mathrm{Cmcm}} = \frac{1}{2}\sum_{k=1}^{n(X_1^+)}\kappa_k^{(X_1^+)}Q_1^+(\mathbf{q}_1)_k^2 + \frac{1}{2}\sum_{k=1}^{n(X_2^+)}\kappa_k^{(X_2^+)}Q_2^+(\mathbf{q}_1)_k^2$$

$$+ \frac{1}{2}\sum_{k=1}^{n(X_4^+)}\kappa_k^{(X_4^+)}Q_4^+(\mathbf{q}_1)_k^2$$

37

$$+\langle Q_3^-(\mathbf{q}_1)\rangle \Bigg[\sum_{k=1}^{n[X_2^+]} \sum_{l=1}^{n[\Gamma_5^-]} a_{k,l}^{(1)} Z_k Q_2^+(\mathbf{q}_1)_l$$

$$+ \sum_{k=1}^{n[X_1^+]} \sum_{l=1}^{n[\Gamma_5^-]} b_{k,l}^{(1)} Y_k Q_1^+(\mathbf{q}_1)_l$$

$$\sum_{k=1}^{n[X_4^+]} \sum_{l=1}^{n[\Gamma_3^-]} c_{k,l}^{(1)} Q_3^-(0)_k Q_4^+(\mathbf{q}_1)_l \Bigg] .$$

$Q_3^-(\mathbf{q}_1)$ is replaced by $\langle Q_3^-(\mathbf{q}_1)\rangle$ leading to a bilinear interaction which mixes new modes.

We will analyze the Z-component of the dipole moment operator. The other components are treated analagously. Due to the mixing of modes, the bare mode operator Z_k is related to the true mode operators (indicated by tildes)

$$Z_k = \tilde{Z}_k + \sum_l \frac{a_{kl}^{(1)} \tilde{Q}_2^+(\mathbf{q}_1)_l}{\kappa_l^{X_2^+} - \kappa_{\perp,k}} \langle Q_3^-(\mathbf{q}_1)\rangle .$$

Thus the Z-component of the dipole moment operator which creates modes $\tilde{Q}_2^+(\mathbf{q}_1)_l$ denoted $p_{Z,Q_2^+,l}$ is

$$p_{Z,Q_2^+,l} = p_{\perp,k} \frac{a_{kl}^{(1)} \langle Q_3^-(\mathbf{q}_1)\rangle}{\kappa_l^{(X_2^+)} - \kappa_{\perp,k}} \langle Q_3^-(\mathbf{q}_1)\rangle , \tag{A1}$$

and the intensity of this induced mode is $|p_{Z,Q_2^+,l}|^2$. The quantities in Eq. (A1) are amenable to a first principles frozen-phonon calculation.

---

[1] S. N. Ruddlesden and P. Popper, Acta Cryst. **11**, 54 (1958).

[2] T. Kimura, T. Goto, H. Shintani, K. Ishizaka, T. Arima, and Y. Tokura, Nature **426**, 55 (2003).

[3] N. Hur, S. Park, P. A. Sharma, J. S. Ahn, S. Guha, and S.-W. Cheong, Nature (London), **429**, 392 (2004).

[4] T. Lottermoser, T. Lonkai, U. Amann, D. Hohlwien, J. Ihringer, and M. Fiebig, Nature (London) **430**, 541 (2004).

[5] S. Kobayashi, T. Osawa, H. Kimura, Y. Noda, I. Kagomiya, and K. Kohn, J. Phys. Soc. Jpn. **73**, 1593 (2004).

[6] G. Lawes, A. B. Harris, T. Kimura, N. Rogado, R. J. Cava, A. Aharony, O. Entin-Wohlman, T. Yildirim, M. Kenzelmann, C. Broholm, and A. P. Ramirez, Phys. Rev. Lett. **95**, 087205 (2004).

[7] M. Kenzelmann, G. Lawes, A. B. Harris, G. Gasparovic, C. Broholm, A. P. Ramirez, G. A. Jorge, M. Jaime, S. Park, Q. Huang, A. Ya. Shapiro, and L. A. Demianets, Phys. Rev. Lett. **98**, 267205 (2007).

[8] N. A. Benedek and C. J. Fennie, arXiv: 1007.1003.

[9] A. B. Harris, arXiv: 1101.2592.

[10] J. M. Perez-Mato, M. Aroyo, A. Garcia, P. Blaha. K. Schwarz, J. Schwiefer, and K. Parlinski, Phys. Rev. B **70**, 214111 (2004).

[11] S. F. Matar, V. Eyert, A. Villesuzanne, and M.-H. Whangbo, Phys. Rev. B **76**, 054403 (2007).

[12] C. Cardoso, R. P. Borges, T. Gasche, and M. Godinho, J. Phys. Condens. Matter **20**, 035202 (2008).

[13] I. D. Fawcett, J. E. Sunstrom IV, M. Greenblatt, M. Croft, and K. V. Ramanujachary, Chem. Mater. **10**, 545 (1955).

[14] L. A. Bendersky, M. Greenblatt, and R. Chen, J. Solid State Chem. **174**, 418 (2003).

[15] N. Guiblin, D. Grebille, H. Leligny, and C. Martin, Acta. Cryst. C **58**, i3 (2002).

[16] M. A. Green and D. A. Neumann, Chem. Mater. **12**, 90 (2000).

[17] Y. L. Qin, J. L. García-Muñoz, H. W. Zandbergen, and J. A. Alonso, Phys. Rev. B **63**, 144108 (2001).

[18] G. Lawes, private communication.

[19] *Isotropy Subgroups of the 230 Crystallographic Space Groups*, H. T. Stokes and D. M. Hatch, (World Scientific, Singapore, 1988).

[20] A. Pimenov, A. A. Mukhin, V. Yu. Ivanov, V. D. Travkin, A. M. Balbashov, and A. Loidl, Nat. Phys. **2**, 97 (2006).

[21] A. Pimenov, T. Rudolf, F. Mayr, A. Loidl, A. A. Mukhin, and A. M. Balbashov, Phys. Rev. B **74**, 100403(R) (2006).

[22] A. B. Sushkov, R. V. Aguilar, S. Park, S.-W. Cheong, and H. D. Drew, Phys. Rev. Lett. **98**,

027202 (2007).

[23] H. Katsura, A. V Balatsky, and N. Nagaosa, Phys. Rev. Lett. **98**, 027203 (2007).

[24] R. Valdes Aguilar, A. B. Sushkov, C. L. Zhang, Y.-J. Choi, S.-W. Cheong, and H. D. Drew, Phys. Rev. B **76**, 060404 (2007).

[25] R. Valdes Aguilar, M. Mostovoy, A. B. Sushkov, C. L. Zhang, Y.-J. Choi, S.-W. Cheong, and H. D. Drew, Phys. Rev. Lett. **102**, 047203 (2009).

[26] A. J. C. Wilson, *International Tables for Crystallography* (Kluwer Academic, Dordrecht, 1995), Vol. A.

[27] *Irreducible Representations of Space Groups*, S. C. Miller and W. F. Love.

[28] The irreps for the X point are two dimensional because they deal with both arms of the star of the wave vector. The first row and column of the irrep matrices refer to wave vector $\mathbf{q}_1$ and the second to $\mathbf{q}_2$. Unlike Ref. 19 we choose the irreps so that the matrices for the translation operators are diagonal.[9]

[29] K. S. Aleksandrov and J. Bartolomé, J. Phys. Condens. Matter **6**, 8219 (1994).

[30] D. M. Hatch, H. T. Stokes, K. S. Aleksandrov, and S. V. Misyul, Phys. Rev. B **39**, 9282 (1989).

[31] It will be observed that the two families can be visualized as resulting from the two equivalent orientations of the original sample which differ by a four-fold rotation. So the two families lead to two equivalent domain structures.

[32] J. R. Ferraro, K. Nakamoto, and C. W. Brown, *Introductory Raman Spectroscopy*, 2nd Ed. (Academic Press, New York, 2003), Ch. 1.

[33] *Raman Scattering in Materials Science*, W. H. Weber and R. Merlin (Eds), (Springer-Verlag, Berlin, 2000), Ch. 1.

[34] C. Fennie and K. Rabe, Phys. Rev. Lett. **96**, 205505 (2006).

[35] A. B. Harris, Phys. Rev. B **76**, 054447 (2007); Phys. Rev. B **77**, 019901(E) (2008).

[36] In fact, Ref. 35 proposed this mechanism to explain the lack of such a correlation seen in experiments. With only magnon-phonon coupling the phonon energy shift in $Eu_{0.75}Y_{0.25}MnO_3$ would be expected to be approximately 20 cm^{-1} whereas it is observed to be only 2 cm^{-1}.[24]

[37] M. Lobanov, M. Greenblatt, El'ad N. Caspi, J. D. Jorgensen, D. V. Sheptyakov, B. H. Toby, C. E. Botez, and P. W. Stephens, J. Phys. Condens. Matter **16**, 5339 (2004).

[38] E. O. Wollan and W. C. Koehler, Phys. Rev. **100**, 545 (1955).